國立臺灣大學醫學院微生物學研究所

碩士論文

Graduate Institute of Microbiology
College of Medicine
National Taiwan University

Master Thesis

NRIP 在神經肌肉接合處可作為乙醯膽鹼受體複合物的結構性蛋白

NRIP is a structural component of AChR cluster complex at neuromuscular junction

賴姿云

Tzu-Yun Lai

指導教授：陳小梨 博士

Advisor: Show-Li Chen, Ph.D.

中華民國 108 年 7 月

July 2019

doi:10.6342/NTU201902676

國立臺灣大學（碩）博士學位論文
口試委員會審定書

中文題目：NRIP 在神經肌肉接合處可作為乙醯膽鹼受體複合物的結構性蛋白

英文題目：NRIP is a structural component of AChR cluster complex at neuromuscular junction

本論文係 賴姿云 君（學號 R06445125 ）在國立臺灣大學微生物學所完成之碩（博）士學位論文，於民國 108 年 07 月 18 日承下列考試委員審查通過及口試及格，特此證明

口試委員：陳小梨（簽名）

（指導教授）

系主任、所長 蔡靜芸（簽名）

doi:10.6342/NTU201902676

致謝

完成這本論文的同時，兩年碩班生活也隨之畫下句點，這一路上接受了很多人的幫助、扶持才能走到這裡。首先謝謝陳小梨老師讓我能在這間實驗室學習，每次的實驗與論文指導都讓我的思考更嚴謹，更了解科學研究的邏輯。另外，老師身為研究學者對學術領域的熱忱令我非常敬佩，我想我學到最重要的是即使實驗的路上充滿失敗的嘗試，還是要秉持著好奇心重新假設並小心的驗證，這樣的態度期許自己在未來的人生中也能不斷學習，謝謝老師這段時間的教誨。謝謝我的口委王培育老師與蔡力凱醫師，每次的進度報告時的討論與建議所激起的反思都讓我的實驗與論文變得更完整，也很感謝三位老師給的鼓勵讓我更有自信，能讓老師們指導是我的榮幸。

在每天的碩班日常裡，我很幸運遇到一群厲害的人們一起努力。謝謝信雄學長，這段時間除了給我實驗上的幫助，從學長身上也學到充滿正能量的實驗態度，讓我不會迷失在實驗失敗的挫折裡，能想著重要的人事物繼續努力。謝謝楚崴學長，學長總是很細心的觀察，在我不知所措的時候給予建議和鼓勵，也感謝學長很勇敢地看完我的漫畫哈哈！希望學長在美國能一切安好。謝謝實驗室女神雅如，從碩一開始就受妳很多照顧，常常跟你借上課筆記到討論實驗，你總是心思縝密的考慮很多實驗的細節，在我實驗不斷失敗的時候給許多建議，再鼓勵我一切會更好的。謝謝你跟我一起走過兩年的風風雨雨，有你一起做實驗、吃飯聊天和捶桌讓實驗生活變得很有趣快樂，祝福你到瑞典交換一切順利！謝謝婉欣，在實驗上的思考與積極度讓我學到很多，在你口試完還假日來教我做 AAV，感恩讚嘆婉大！謝謝韻心，你做實驗的效率與精確度讓我很憧憬，畢業後我還是常常打擾問你動物實驗的問題，感謝你總有耐心的幫助我。謝謝首領詩浩，在我開始克隆的時候給我很多的幫助，你做實驗豁達但不失謹慎的態度也讓我覺得佩服。謝謝伯翰，你對實驗總是特別仔細與認真，身為實驗室的暖男常常關心與鼓勵我們各種大小事，對不起啦碩一時常常消費你，有你在的 R710 就特別溫暖快樂。謝謝亦翔，和你討論實驗的過程中我學到很多，你會是一個很棒的科學家的，但把 AChRγ 交給你真是特別抱歉嗚嗚。謝謝婉恩，一起討論 confocal 的時候讓我思考了很多新想法，有你在的實驗室就很歡樂。謝謝亦欣總是很貼心，我相信你們之間是真的沒有裂縫的。謝謝釗昕，手很巧的你常常給實驗室生活上的小驚喜，也會幫忙解決困難。謝謝浩文，雖然平常看似安靜但只要講話就會很有趣，其實也是默默關心著大家。感謝碩一的你們帶給我們的種種歡樂與驚喜，R710 以後就是你們的天下啦。

最後要感謝我的家人，謝謝他們讓我我任性的再多讀兩年書，爸爸在每個做實驗很晚的日子都會等我並載我回家，而媽媽總是會關心我忙碌之餘的身體健康，從小到大他們都始終如一的陪伴在我身邊給我鼓勵與支持，謝謝你們，小女我真的要畢業了！這兩年來所獲得的比我當初想像的多太多了，是你們的幫助才讓我走到這裡。我會帶著這些點點滴滴與收穫繼續在人生的道路上奔跑著，期待這些讓我繼續成長，也期待我們在未來、在某片天空下再次相遇。

doi:10.6342/NTU201902676

中文摘要

在神經肌肉接合處(neuromuscular junction, NMJ)的發展上，agrin-Lrp4-MuSK 信號會促使乙醯膽鹼受體(acetylcholine receptors, AChRs)在肌肉細胞膜上形成緊密的聚集，以此形成功能良好，能有效率接收訊號的神經肌肉接合處。乙醯膽鹼受體由 α, β, γ, δ 四個子單位構成，在內質網形成 α2βγδ 的聚合體並以此型態表現在肌肉細胞膜上。Rapsyn 為近細胞膜蛋白，可以和乙醯膽鹼受體有直接交互作用並促使乙醯膽鹼受體在神經肌肉接合處形成聚集。缺乏 rapsyn 的小鼠神經肌肉接合處上的乙醯膽鹼受體無法形成聚集，導致老鼠無法存活。另外，輔肌動蛋白異構體 (α-actinin 2, ACTN2) 在神經肌肉接合處與 rapsyn 有直接交互作用，在 agrin 的調控下 ACTN2-rapsyn 也會影響乙醯膽鹼受體聚集。因此，rapsyn, ACTN2 與乙醯膽鹼受體三者為目前已知的乙醯膽鹼受體複合物 (AChR complex)。核受體交互作用蛋白(Nuclear receptor interaction protein, NRIP)是一個鈣離子依賴性的攜鈣素(calmodulin)結合蛋白，其中涵蓋 7 個 WD domain 與 1 個 IQ domain。在本實驗室先前的研究中，全身性 NRIP 基因剃除小鼠有肌肉失養及受損的運動能力。另外 在 16 周大的肌肉 NRIP 基因剃除小鼠中觀察到神經肌肉接合處的異常，包括神經肌肉接合處的面積減少和神經支配比例(軸突神經支配/去神經支配的比例 (axonal innervtion/denervation))，和運動神經元(α-motor neuron)退化。這代表 NRIP 可能參與在神經肌肉接合處的行程與維持之中。在先前研究我們發現 NRIP 可以透過自身的 IQ domain 與 ACTN2 的 EF-hand 有交互作用。鑑於 ACTN2 為乙醯膽鹼受體複合物的一員，加上我們所觀察到的 NRIP 對神經肌肉接合處的影響，我們推測 NRIP 可能也是組成乙醯膽鹼受體複合物的結構性蛋白。透過免疫螢光染色我們觀察到 NRIP 是一個近膜蛋白，且與 rapsyn、ACTN2 與乙醯膽鹼受體共定位(co-localize)在肌肉細胞膜上。使用免疫沉澱法(Immunoprecipitation) 也看到 NRIP 與 rapsyn、ACTN2 可以共同被乙醯膽鹼受體沉澱下來，因此代表 NRIP 是乙醯膽鹼受體複合物之中的一個結構性蛋白。

我們進一步想探討 NRIP 與乙醯膽鹼受體是如何進行交互作用的。我們使用免疫沉澱法觀察到 NRIP 可與乙醯膽鹼受體的 α, β 和 δ 子單位有交互作用，並使用不同片段的 NRIP 觀察到在把 NRIP 的 WD7 domain 去除後，NRIP 便無法和 AChR-α 結合。因此可以得知 NRIP 是透過 WD7 domain 來與 AChR-α 有交互作用。為了瞭解 NRIP 與乙醯膽鹼受體的交互作用與促進乙醯膽鹼受體聚集產生是否有關連，我們共轉染 EGFP-NRIP 不同片段和 mCherry-α 再以共軛焦顯微鏡觀察乙醯膽鹼受體聚集產生的情形。結果顯示和 AChR-α 有交互作用的片段，包括 NRIP-FL 與 NRIP-C 皆可使 AChR-α 在細胞內產生許多的聚集。而 C-ΔWD7 在先前沒有看到與 AChR-α 有交互作用，在此實驗也觀察到較少的 AChR-α 聚集。這顯示 NRIP 透過 WD7 domain 和 AChR-α 的交互作用與 AChR-α 形成聚集是有相關的。

最後，我們想知道在細胞觀察到的 AChR-α 聚集形成與生物體內神經肌肉接合處的行成是否有相關性。我們使用肌肉注射給予帶有 NRIP-C 與 C-ΔWD7 基因的相關腺病毒(AAV)進行基因治療，觀察肌肉 NRIP 基因剃除小鼠的神經肌肉接合處的

doi:10.6342/NTU201902676

形成是否會受到影響。先前實驗室研究結果顯示給予 AAV-NRIP 基因治療可以顯著改善使神經肌肉接合處型態正常與運動神經元的存活。我們使用肌肉注射給予 AAV-NRIP-C 與 AAV-C-ΔWD7 基因治療，並觀察到 AAV-NRIP-C 可以改善肌肉 NRIP 基因剃除小鼠的神經肌肉接合處的面積減少和神經支配比例，也改善與運動神經元的存活率，而 AAV-C-ΔWD7 則無法。因此我們知道 NRIP 透過 WD7 domain 和 AChR-α 的交互作用與神經肌肉接合處的完整和運動神經元的退化死亡有相關。綜合上述所發現的，NRIP 是乙醯膽鹼受體複合物之中的一個結構性蛋白，透過 WD7 domain 與乙醯膽鹼受體有交互作用並參與神經肌肉接合處的乙醯膽鹼受體聚集形成，藉此影響神經肌肉接合處的形成與穩定。

關鍵詞：核受體交互作用蛋白；神經肌肉接合處；乙醯膽鹼受體；基因治療; WD40 domain

doi:10.6342/NTU201902676

Abstract

Synapses formed between motor neurons and skeletal muscle fibers are named neuromuscular junction (NMJ). During development of neuromuscular junction (NMJ), agrin-Lrp4-MusK signaling pathway regulates acetylcholine receptors (AChRs) to form dense clusters at postsynaptic muscle membrane, which are essential for well function NMJ. AChR are consist of α, β, γ, δ four subunits and assembles to pentamer as $\alpha_2\beta\gamma\delta$ at ER, then transport and localized on membrane. Rapsyn, a 43kDa peripheral membrane protein, is known to bind directly to AChR subunits and participate in AChR cluster formation through its binding ability. Mice with absence of rapsyn would cause failure AChR clustering at NMJ and mice died perinatally. Moreover, ACTN2 interacts with rapsyn directly at NMJ. With agrin's regulation, rapsyn-ACTN2 also take part in AChR clustering in NMJ. Taken together, AChR-rapsyn-ACTN2 form a ternary complex on muscle membrane, components of AChR complex are associate with AChR clustering and NMJ formation. Nuclear receptor interaction protein (NRIP) is a Ca^{2+}-dependent calmodulin-binding protein, consists of 860 amino acids and containing seven WD-40 repeats and one IQ motif. In our previous study, NRIP global knockout (gKO) mice show muscle dystrophy and impaired motor function. Furthermore, muscle specific NRIP knockout (cKO) mice demonstrate NMJ abnormality with decreased NMJ area and axonal denervation, loss of motor neuron in spinal cord and motor function defects at

doi:10.6342/NTU201902676

adult age (16week). These indicates that NRIP may play a role in NMJ formation and maintenance. In previous study we also investigated that NRIP can interact with ACTN-2 EF-hand through its IQ domain. Since ACTN2 is a component of AChR complex, combined NRIP's influence at NMJ, we hypothesis that NRIP is a structural component of AChR and participate in AChR clustering at NMJ. By immunofluorescence assay, we examined that NRIP is a membrane bound protein and colocalized with rapsyn, ACTN2 and AChR at cell membrane. NRIP can also be pulled down with ACTN2 and rapsyn by AChR. These indicates that NRIP is a novel structural component of AChR complex.

To further discuss how NRIP bind with AChR, we performed immunoprecipitation and examined NRIP can bind to AChR α, β and δ with different affinity. On the other hand, NRIP loss AChR-α binding ability when WD7 domain were truncated, indicating that NRIP and AChR-α is reciprocally interaction through WD7 domain. To investigate whether NRIP's binding ability to AChR is associated with AChR cluster formation, we co-transfected EGFP-NRIP mutants and mCherry-AChR-α into HEK293T cells, examined cluster formation in cells by confocal microscopy. The result shows that NRIP mutants that have binding ability to AChR-α can form AChR clusters in cells, while C-ΔWD7, which loss binding ability to AChR-α, cannot form AChR clusters. Taken together, WD7 domain of NRIP is responsible for AChR-α binding, and this interaction is essential for AChR cluster formation.

doi:10.6342/NTU201902676

Last, to see whether the ability of AChR cluster formation in cells can represent AChR clustering in vivo, we examine NMJ formation by given gene therapy of AAV-NRIP-C and AAV-C-ΔWD7 to 6weeks-old NRIP cKO mice. Our previous study showed AAV-NRIP treated cKO mice had improved NMJ integrity and motor neuron survival. Here we performed gene therapy of AAV-NRIP-C and AAV-C-ΔWD7 by intramuscular injection and the results show that AAV-NRIP-C can increase NMJ area size, axonal denervation, and enhance motor neuron survival in NRIP cKO mice, while AAV-C-ΔWD7 cannot. Collectively, NRIP WD7 domain's AChR binding ability is responsible for NMJ formation, as well as motor neuron degeneration. To sum up, NRIP is a novel structural component of AChR complex, participates in AChR clustering at NMJ formation and stabilization through its binding with AChR by WD7 domain.

Keywords: NRIP; neuromuscular junction; acetylcholine receptor; gene therapy; WD40 domain

doi:10.6342/NTU201902676

Table of contents

doi:10.6342/NTU201902676

doi:10.6342/NTU201902676

doi:10.6342/NTU201902676

Chapter 1 Introduction

1.1 Nuclear receptor interaction protein (NRIP)

Previously, we found nuclear receptor interaction protein (NRIP) that isolated by yeast two-hybrid system using androgen receptor (AR) as the bait to screen human HeLa cDNA library (Tsai et al., 2005); NRIP is also named as IQ motif and WD repeats 1 (IQWD1) (Nakano et al., 2013)or DDB1 and CUL4 associated factor 6 (DCAF6) (Jin et al., 2006). NRIP consists of 860 amino acids, containing seven WD-40 repeats (conserved structural motif of 40 amino acids, often terminating in tryptophan-aspartic aid dipeptide) and one IQ motif (Chang et al., 2011; Tsai et al., 2005). NRIP is an androgen receptor (AR) interaction protein to enhance androgen receptor (AR) and glucocorticoid receptor (GR) mediated transcriptional activity (Chen et al., 2008). Knockdown of endogenous NRIP in cervical cells (C33A) and prostate cancer cells (LNCaP) reduces cell proliferation, indicates NRIP may influence development of cervical cancer and prostate cancer (Tsai et al., 2005). The role of NRIP in human cervical cancer, NRIP can stabilize human papillomavirus E2 protein through its IQ domain, which is known as $Ca2^{+}$/calmodulin (CaM) binding domain, to recruit calcineurin by interacting with CaM to dephosphorate HPV-E2 (Chang et al., 2011); indicating that NRIP involves in human cervical cancer. Furthermore, the increased levels of AR and NRIP in human prostate cancer tissues compared to non-neoplastic prostate tissues, revealed that NRIP is associated with

doi:10.6342/NTU201902676

prostate cancer (Chen et al., 2017). The recruitment of NRIP to AR is also associated with adverse clinical outcomes in breast cancer cases, which immunohistochemistry of whole breast cancer tissue sections revealed relative high levels of NRIP (Nakano et al., 2013). In other study also showed NRIP can be detected in tissue samples of several types of tumors by tissue microarray (TMA) for example—cancers; NRIP expression with high specificity in neoplastic tissues compared to non-neoplastic healthy tissue, can be used for cancer confirmation in immunohistochemistry (IHC) (Han et al., 2008). NRIP genome location at [Chr1q24.2], from genetic variation analysis such as single nucleotide polymorphism (SNP), NRIP is associated with osteoporosis, schizophrenia and cardiovascular disease (Cheung et al., 2009; Ehret et al., 2009; Shi et al., 2011). Taken together, NRIP participates in several human diseases.

1.2 NRIP regulates muscle contraction and regeneration.

NRIP contains seven WD-40 domains and one IQ motif according to SMART database (http://smart.embl-heidelberg.de/) (Chang et al., 2011). IQ motif had been reported to bind to calmodulin (CaM) or EF-hand protein, which contains EF hand domain or motif and forms a four helix bundle domain that can binds to Ca^{2+}, in a Ca^{2+} dependent manner (Bhattacharya et al., 2004). IQ motif mostly presents in vertebrate's myosin and neuronal proteins, like cardiac myosin beta in human and neuromodulin in bovine for example

doi:10.6342/NTU201902676

(Bahler and Rhoads, 2002; Rhoads and Friedberg, 1997). NRIP can activate calcineurin (CaN) and CaMKII through binding with CaM by its IQ motif to activate CaN. The activated CaN can dephosphorylate cytosol nuclear factor of activated T-cells cytoplasmic calcineurin-dependent 1(NFATc1). The dephospho-NFATc1 then translocates into nucleus to induce repression of MyHC-2B and induction of MyHC-slow, resulting muscle-fiber-type switch to a slow-twitch and oxidative phenotype (Calabria et al., 2009; Chen et al., 2015; Chin et al., 1998). Previously we generated global NRIP knockout (gKO) mice to delete NRIP gene in all tissues, show the decreased muscle strength and delayed skeletal muscle regeneration after injury due to the impaired CaN-NFATc1 signaling compared with age-match wild type mice. Additionally, gKO mice show the decreased of slow myosin expression and mitochondrial activities; as well as the reduced level of Ca^{2+} storage in sarcoplasmic reticulum (SR) those may correlate with muscle contraction (Chen et al., 2015). In muscle specific NRIP knock out (cKO) mice that delete NRIP expression in skeletal muscle tissue, we examined decreased expression of slow myosin and mitochondrial activities, as well as impaired motor function at age 16 weeks (Chen et al., 2018). Thereof, NRIP regulates slow myosin gene expression, mitochondrial function, muscle regeneration through CaN-NFATc1 signaling and influence motor function, plays an important role in muscle contraction.

doi:10.6342/NTU201902676

1.3 Characteristics of neuromuscular junction (NMJ)

Nervous system activities are seen between neuron-neuron or neuron with its targeted cells (such as muscle cells). Synapses formed between motor neurons and skeletal muscle fibers are named neuromuscular junction (NMJ). High densities of neurotransmitter receptors, such as acetylcholine receptors (AChRs), are packed on postsynaptic muscle membranes (Wu et al., 2010). Initially, AChRs are evenly distributed on mouse aneural muscle fibers. During early embryonic stage (E12.5 to E14.5), motor neurons start to innervate to primary myotubes and cause AChRs accumulate in a central region where motor axon innervates (Tintignac et al., 2015; Wu et al., 2010; Ziskind-Conhaim and Bennett, 1982). During motor neuron innervating muscle cells, agrin-lipoprotein receptor related protein 4 (Lrp4)-muscle specific tyrosine kinase receptor (MuSK) pathway is the best characterized signaling regulates vertebrates AChR assembly. The glycoprotein agrin is synthesized in motor neuron and released to basal lamina, which surrounds the muscle fiber (Campanelli et al., 1991; Ruegg and Bixby, 1998). Agrin released from motor neuron binds to Lrp4, an agrin co-receptor, then promotes MuSK autophosphorylation and activation. The phosphorylated Musk activates signaling pathways, such as rapsyn, that induces phosphorylation and clustering of AChRs at presynaptic muscle membrane (Kim et al., 2008; Zhang et al., 2008). Following agrin-Lrp4-MuSk signaling pathway induced AChR clustering, the innervated clusters are enlarged, while primitive clusters disappear

doi:10.6342/NTU201902676

in synaptic and extrasynaptic regions at E18.5 (Lin et al., 2001; Yang et al., 2001). With AChR clusters form by agrin-Lrp4-MuSK, neurotransmitter acetylcholine (ACh), which is released from presynaptic motor neuron as a reaction to action potential, is able to bind with dense AChR clusters on muscle membrane and induce rapid synaptic transmission (Burden et al., 2018). In mature muscle, each myofiber is innervated by a single motor axon ultimately (Burden et al., 2018). Thus, innervation and clustering of AChRs are essenial in a well-function NMJ.

1.4 AChR subunits structure and cluster formation

AChR, localized on muscle membrane, is a ligand-gated binding ionic channel which binds to neurotransmitter acetylcholine (ACh). It was first purified by α-bungarotoxin (α-BTX), a component of krait snake venom that binds to muscle type AChR (Barnard et al., 1977). AChR is a muscle membrane intergrated protein, consists of 4 different yet homologous subunits (α, β, γ, δ) that assembles into a pentamer with a stoichiometry of $\alpha_2\beta\gamma\delta$ with molecular weight ~270 kDa (embryonic γ subunit will be replaced by ε subunit in adult human muscle) (Green and Claudio, 1993; Unwin, 2013). Four subunits are the separated gene products, which folding and assembling in or on the surface of endoplasmic reticulum (ER) into native AChR that compose of $\alpha_2\beta\gamma\delta$ (Green and Claudio, 1993; Wanamaker et al., 2003). All subunits have four common structural domains: (1)

doi:10.6342/NTU201902676

~200 amino acid of conserved extracellular large NH2-terminal domain; (2) three prominent and conserved transmembrane (TM) domain; (3) one cytoplasmic loop with variable size and amino acid sequence; (4) a fourth TM domain with a relatively short and variable extracellular COOH-terminal sequence (Albuquerque et al., 2009; Unwin, 2013) (Supplementary Fig.S1). Four subunits are further classified to α- and non α-subunits depending on presence of a cysteine–cysteine (Cys-Cys) pair, which is required for agonist binding, near the entrance of TM1. The Cys-Cys pair is essential for agonist binding and its presence identified the subunit as α- subunit (Karlin et al., 1986; Lukas et al., 1999). Compared to extracellular NH2-terminal domain, intracellular domain contributes to protein-protein interactions that involves in AChR assembly, subcellular localization and stabilization (Kracun et al., 2008). The Agrin-Lrp4-Musk signaling pathway phosphorylate MuSK. Activated MuSK further phosphorylate AChR β subunit, AChRs are clustered via rapsyn's binding to AChR and cytoskeletal protein. In fetal muscle, Agrin-Lrp4-Musk signaling pathway anchored AChR clusters to motor axonl terminal (Borges et al., 2008). 4 subunits of AChR assembles into $\alpha_2\beta\gamma\delta$ pentamer in ER, then traffics to muscle membrane through Golgi and post Golgi vesicles. The AChR clustering region on post synaptic muscle membrane first formed as a small, plaque shape, then enlarge and forms a pretzel-like arrays that match to pre-synaptic branches precisely on muscle membrane (Marchand et al., 2002; Marques et al., 2000; Sanes and Lichtman,

doi:10.6342/NTU201902676

1999; Steinbach, 1981).

1.5 The role of rapsyn in AChR cluster formation

Rapsyn is a 43kDa peripheral membrane protein which first discovered by large-scale purification of membrane fragment in AChR in Torpedo (Cohen et al., 1972; Sobel et al., 1977). Rapsyn locates on muscle membrane plays an important role in NMJ maintenance and stabilization of AChR clustering (Burden et al., 2018; Wu et al., 2010). Rapsyn contains seven tetratrichopeptide (TPR) repeats, myristoylated N-terminal, a coiled-coil domain and RING finger domain C-terminal (Bartoli et al., 2001; Ramarao et al., 2001). Rapsyn co-localized with AChR at the early stage of innervation as well as the adult NMJ (Froehner et al., 1990; Noakes et al., 1993). Previously, the compelling evidences showed the rapsyn's AChRs cluster ability in cells; when co-transfection of AChR and rapsyn would induce AChR clustering in cytoplasm and cell membrane in QT-6, COS7, and HEK-293T cells; implying that rapsyn have ability to induce formation of AChR clusters in non-muscle cells (Phillips et al., 1991; Ramarao and Cohen, 1998; Yu and Hall, 1994). The myristolation of N-terminal of rapsyn contributes to itself targeting to cell membrane, while coiled-coil domain of rapsyn is necessary for inducing AChR cluster formation (Musil et al., 1988; Ramarao and Cohen, 1998). The RING finger domain of rapsyn contains E3 ligase activity, which regulates AChR neddylation and induces AChR

doi:10.6342/NTU201902676

clustering and NMJ formation (Li et al., 2016). For participating in AChR clustering, rapsyn is found to bind four AChR subunits and have interaction with postsynaptic cytoskeleton such as α-actinin, through microtubule actin cross linking factor's (MACF) actin binding site (ABD) on postsynaptic muscle membrane(Antolik et al., 2007; Neubig et al., 1979; Oury et al., 2019). Once receive agrin's stimulation from presynaptic neuron, AChR β subunit on postsynaptic muscle membrane becomes tyrosine phosphorylated following by MuSK activation. The phosphorylated AChR β subunit recruits rapsyn, further induce more AChR clusters that bind with rapsyn to gather (Borges et al., 2008; Lee et al., 2009). The in vitro study of non-muscle cells indicates that rapsyn traffics to cell membrane through exocytic pathway along with pentamer-AChRs, leading more AChR express on HEK293T cell membrane compare with non-rapsyn group, implying that rapsyn is necessary for AChR's membrane targeting (Marchand et al., 2002). In vivo study shows that the absence of rapsyn caused failure of AChR clustering and mice died perinatally (Apel et al., 1997; Banks et al., 2001).

1.6 The role of α-actinin2 (ACTN2) in NMJ

The cytoskeletons consist of polymers of actin, tubulin and intermediate filament protein. α-actinin belongs to spectrin superfamily, can crosslink actin filament into bundles. 4 kinds of actinin protein is classified into 2 classes, actinin 2 and 3 are muscle isoforms

doi:10.6342/NTU201902676

while actinin 1 and 4 are non-muscle isoforms that are associated with stress fiber (Sjoblom et al., 2008). that α-actinin 2 (ACTN2) is a major isoform expresses in cardiac and skeletal muscle and ACTN3 expresses in glycolytic skeletal muscles (Mills et al., 2001). Beside α-actinin interaction with actin filament, it appears to be a platform for protein-protein interaction with cytoskeletal and regulatory protein, such as CAMKII and densin, and transmembrane domain, such as ICAM-2 (Heiska et al., 1996; Walikonis et al., 2001). Thus, α-actinin is able to support clustering as well as structural stability via its interaction between transmembrane protein and actin cytoskeleton (Otey and Carpen, 2004; Sjoblom et al., 2008). At NMJ, ACTN2 interacts with rapsyn directly and can be regulated by agrin to form AChR-rapsyn-ACTN2 ternary complex on muscle membrane. Repression of ACTN2 expression in muscle cells impaires agrin-induced AChR clustering on membrane, indicating that rapsyn-ACTN2 interaction takes part in AChR clustering in NMJ (Dobbins et al., 2008).

1.7 Neuromuscular junction impairment in myasthenia gravis (MG) and Congenital myasthenic syndromes (CMS)

There are several diseases that are associate with defects of NMJ formation and maintenance. For example, myasthenia gravis (MG) is an autoimmune disease that causes neuromuscular junction disorder. Patients with MG have fatigable muscle weakness cause

doi:10.6342/NTU201902676

by presence of autoantibodies against NMJ component (Berrih-Aknin et al., 2014). 85% patients of MG present AChR antibody, which binds directly to AChR and causes degradation of AChRs (Drachman et al., 1978). Other MG patients also have antibodies against MusK, agrin and Lrp4, which are crucial for AChR clustering and NMJ maintenance (Gilhus and Verschuuren, 2015). Besides MG, Congenital myasthenic syndromes (CMS) are inherited disorders with impaired neuromuscular transmission by one or more specific mechanisms. CMS usually are onset at birth to early childhood, with fatigable weakness especially affecting the ocular and other cranial muscle (Engel et al., 2015). The common causes of CMS are mutations occur in AChR subunits, mostly ε subunits, result in number of AChRs decrease and further reduce synaptic response to ACh; or mutation in genes that encode protein composing neuron muscular junction, such as MUSK, AGRN, LRP4, DOK7 and RAPSYN, and cause defects of NMJ development and maintenance (Engel et al., 2015). The deficiency of MuSK, agrin, Lrp4, Dok7 and rapsyn's gene further influence their protein expression, lead to impaired agrin-MusK-Lrp4 signaling and interfere AChR clustering and NMJ maintenance (Huze et al., 2009; Maselli et al., 2010; Ohkawara et al., 2014; Ohno et al., 2002). Hence, each component at NMJ, such as MuSK, agrin, Lrp4 and rapsyn are essential for AChR clustering on postsynaptic muscle membrane. Diseases with defects of these NMJ components cause failure in NMJ structural maintenance, further influence skeletal muscle's function in

doi:10.6342/NTU201902676

human.

1.8 The role of NRIP in neuromuscular junction

The interaction between motor neuron and skeletal muscle is bidirectional in NMJ (Boillee and Cleveland, 2004). As motor neurons maintain NMJ integrity and drive muscle contraction, muscle provides trophic factor to support innervation and motor neuron survival (Boillee and Cleveland, 2004; Cary and La Spada, 2008; Kanning et al., 2010; Tsitkanou et al., 2016). Several muscle derived factors can support motor neuron growth and remodeling of its innervation, such as neurotrophin-4 (NT-4) and bone morphogenetic protein (BMP) (Chou et al., 2013; Funakoshi et al., 1995). Besides, MyoD and myogenin, myogenic transcription factors, are muscle regulatory factors that participate in muscle development and differentiation (Park et al., 2013). In our previous study, muscle-specific NRIP conditional knockout (cKO) mice show muscle weakness with abnormal NMJ architecture and axonal denervation at 16 weeks compared with WT. NRIP can induce myogenin, when overexpressing myogenin in NRIP cKO can rescue the phenotypes of abnormal NMJ (Chen et al., 2018). This indicates that NRIP is a trophic factor that can support NMJ stabilization by regulating myogenin expression.

1.9 Aims of the study

doi:10.6342/NTU201902676

In our previous study, we observed the decreased NMJ area and denervation of motor neuron at age 16 weeks of cKO mice. Besides, NRIP is not only co-localized with myogenin but also AChR clusters at NMJ using immunofluorescence assay (Chen et al., 2018). Moreover, NRIP can interact with ACTN-2 EF-hand through its IQ domain (Szu-Wei Chang and Ssu-Yu Lin thesis unpublished result). ACTN-2 is known as a part of AChR complex components (Dobbins et al., 2008). Due to NRIP's influence in NMJ and binding ability to ACTN2 (unpublished results), we raised a hypothesis that NRIP may be an AChR binding protein and participate in AChR clustering formation in cells to impact NMJ formation in mouse model. Firstly, we would improve NRIP as a structural component of AChR complex by immunoprecipitation, like rapsyn (Marchand et al., 2002). In addition, we would analyze whether NRIP interacting with AChR is correlated with AChR cluster formation in cells by immunofluorescence assay; and evaluate NMJ formation in NRIP cKO mouse model by given AAV-NRIP mutants gene therapy to correlate cluster formation in cells.

doi:10.6342/NTU201902676

The aims of this study are following:

1. **To determine whether NRIP is a membrane-bound AChR associated protein.**
2. **Mapping NRIP domain is responsible for AChR binding.**
3. **To determine whether binding between NRIP and AChR is correlated with AChR cluster formation in cells.**
4. **To determine whether AChR cluster formation in cells is correlated with NMJ formation in NRIP cKO mouse model.**

doi:10.6342/NTU201902676

Chapter 2 Materials and methods

2.1 Cell culture

HEK293T cells are cultured in DMEM (Dulbecco's modified Eagle's medium) containing 10% fetal bovine serum, 2mM L-glutamine and 1% penicillin-streptomycin (Thermo Fisher), incubated in 37℃, 5% CO_2.

2.2 HEK233T cell transfection

One day before transfection, seed $1*10^6$ 293T cells in 10cm dish to achieve ~70-80%. We used jetPRIME® (polyplus) to transfect plasmids into cells. The ratio between DNA and jetPRIME reagent is 1:2 or 1:3, total DNA is 10-15 μg/plate. Incubate the cells 24-48 hours post transfection.

2.3 Protein extraction and western blot

The total protein of 293T cells were extracted by RIPA lysis buffer (20mM Tris-HCl pH8.0, 137mM NaCl, 2mM EDTA, 1% NP-40) with 1% protease inhibitors (Roche) and 1% phosphatase inhibitor cocktail 2, 3 (Sigma), incubate on ice for 20 minutes. Protein lysate were clarified by centrifugation at 13,200 rpm for 25 minutes at 4℃, the supernatant was collected and stored in -80℃. Protein samples were separated on 10% SDS-PAGE Electrophoresis system then transferred to PVDF membranes (Millipore).

doi:10.6342/NTU201902676

The membrane was blocked in 5% bovine serum albumin (BSA) for 1 hour in room temperature, then incubated with primary antibodies anti-GFP (ab183734, Abcam, 1:10000), anti-FLAG (F3165, Sigma, 1:10000) amd anti-GAPDH (YIF-LF-PA0212, AbFrontier, 1:10000) diluted in blocking buffer, incubated overnight at 4℃. Target protein expression was detected using an ECL western blot detection system (PerkinElmer).

2.4 Immunoprecipitation

293T cells were transfected with 10μg pEGFP-NRIP or NRIP mutants, 1μg FLAG-AChR-α, p3XFLAG-CMV14 and pEGFP as internal control by jetPRIME transfection reagent (Polyplus). Cells were harvested 48 hours after transfection. Equal amount of protein lysates were incubated with adjust lysis buffer and antibody as mentioned at 4℃ overnight. 30μl Protein G Sepharose (GE Healthcare) beads were added to lysates and incubated at 4℃ for 2 hours. Wash the beads gently with lysis buffer (in the absent or present of 0.1% SDS) for 3 times. Targeting protein were eluted by 5X sample dye and following performed Western blot.

2.5 Immunofluorescence assay of cells

293T cells were seeding on cover-glass one day before transfection. Cells were

doi:10.6342/NTU201902676

transfected with indicated plasmids by jetPRIME and incubated for 24 or 48 hours. The cells were rinsed with phosphate-buffered saline (PBS) three times. For immunofluorescence assay without antibody labeling, cells were fixed and permeabilized by ice cold methanol 5 minutes. After 3 times 10 minutes' washes with PBS, the cover-glass were picked and mounted in DAPI Fluoromount-G (SounthernBiotech, Birmingham, AL, USA). For immunofluorescence assay that required antibodies labeling, cells were fixed in 2% para-formaldehyde (PFA) for 10~15 minutes, then washed with PBS for 3 times. Samples were then permeabilized by ice cold methanol 5 minutes, following washed with PBS for 3 times. Cells were blocked with 2% BSA in PBS for one hour at room temperature, then incubated with primary antibodies 4℃ overnight: anti-FLAG (F3165, Sigma), anti-GFP (sc-9996, Santa Cruz). After three 10-minuites washed with PBS, samples were stained with fluorescent secondary antibodies for 1 hour at room temperature and mounted in DAPI. For Wheat-germ agglutinin (WGA) staining for cell membrane, WGA were stained after 2% PFA fixed for 1 hour. Immunostained samples were analyzed by Carl Zeiss LSM880 confocal microscope.

2.6 AAV production

The gene fragment including EGFP-NRIP-C and EGFP-NRIP-CΔWD7 was amplified by PCR using pEGFP-NRIP-C and pEGFP-NRIP-CΔWD7 as template. The product was

doi:10.6342/NTU201902676

then digested by BamHI and SalI and ligased into AAV-MCS vector under control of Human cytomegalovirus (CMV) promoter which is done by Szu-Wei Chang. For production of AAV-NRIP-C and AAV-C-ΔWD7, HEK293T cells were co-transfected with p AAV-NRIP-C or p AAV-C-ΔWD7, pAAV-DJ/8 and the adenovirus helper plasmid pHelper by calcium phosphate transfection and cultured for 72 hours. Cell lysates were harvested and lysed by freeze-thaw cycle, cause viruses to release to supernatant. The AAV particles were purified by CsCl density-gradient ultracentrifugation and dialyzed by dialysis cassette (Slide-A-Lyzer dialysis cassettes, Thermo; MWCO 10K) in dialysis buffer containing 350 mM NaCl with 5% sorbital in 1X PBS at 4℃. The viral titers were determined by dot blot assay. Virus were separated into small portions and stored at -80℃ until future used.

2.7 Muscle-specific NRIP knockout mice

The generation of muscle-specific NRIP knockout mice was described in previous study (Chen et al., 2015). Mouse NRIP genomic DNA (bMQ134h07) was obtained by screening a BAC library derived from mouse strain 129, which is a 19.2 kb mouse genomic DNA fraction inserted at the *NotI-SpeI* site of pL253, MC1-TK (thymidine kinase) gene that served as negative selection marker. The resulting construct was used as the backbone for subsequent insertion of loxP sequence from pL452 into intron 1. The final targeting

doi:10.6342/NTU201902676

construct contained a homologous short 5' arm of 4.3 kb and long 3' arm of 10.6 kb. The targeting vector was linearized by DNA digestion with *NotI* (unique site) and electroporated into embryonic stem (ES) cells, and then G418-resistant clones were selected. The ES cells containing the floxed NRIP allele were injected into blastocytes of C57BL/6JNarl mice and implanted into pseudo-pregnant foster mothers. The chimeric offspring was back-crossed to the C57BL/6Jnarl mice (more than 10 generations) to generate the NRIP-LoxP heterozygous ($NRIP^{flox/+}$) mice. To obtain muscle-specific knockout animals, $NRIP^{flox/+}$ mice were crossed with MCK (muscle creatine kinase)-Cre heterozygous mice (Bruning et al., 1998), then the $NRIP^{flox/+}$; MCK-Cre^{+} offspring were crossed with each other to generate $NRIP^{flox/flox}$; MCK-Cre^{+} mice (muscle-specific NRIP knockout mice). Other littermates were used as wild type (WT) controls.

2.8 In vivo AAV injection

Mice were anaesthetized by intraperitoneal injection of 2.5% avertin (200~300 μl). AAV virus were given by intramuscular injection into each bilateral gastrocnemius and tibialis anterior muscles at age 6 weeks. The therapeutic were analyzed for NMJ integrity, axonal denervation and motor neuron survival 10 weeks after gene therapy.

2.9 Frozen section preparation of mice spinal cord and gastrocnemius

doi:10.6342/NTU201902676

Mice were anesthetized with 2.5% avertin and sacrificed by heart excision. For spinal cord, the vertebral column was carefully dissected from thoracic T1 segment to the base of the tail. The paravertebral muscles were removed, and spinal cord were flushed out from the vertebral fraction by PBS with the needle/syringe technique. Searched for the vertebral foramen at the lower part. When the opening is identified, the tip of the needle was inserted in the spinal canal and push the plunger of the syringe containing 1X PBS to flush out spinal cord at the thoracic end. Fresh lumbar segment (L3-L5) of spinal cord was incised and embedded into O.C.T. compound immediately. The O.C.T. block was frozen in isopentane pre-cooled with liquid nitrogen and stored at -80℃. The 30μm thickness serial frozen cross-sections of spinal cord from lumbar L5 segment were prepared by cryostat microtome for immunofluorescence assay. For gastrocnemius, the fresh gastrocnemius muscle dissected from mice was covered with 2% PFA for 2 hours at room temperature. Wash the muscles with 1X PBS 10 minutes for 3 times, then dehydrate with 30% sucrose in PBS and incubate at 4℃ overnight. Dehydrated tissues were then embedded in O.C.T. compound, then frozen in isopentane pre-cooled with liquid nitrogen and stored at -80℃. The 30μm thickness frozen cross-section of GAS were prepared by cryostat microtome for immunofluorescence assay.

2.10 Immunofluorescence assay of neuromuscular junction (NMJ)

doi:10.6342/NTU201902676

The 30μm thickness frozen cross-sections of GAS were wash and then fixed by 2% para-formaldehyde. Wash the slide 10 minutes in 1X BS for three times and incubated with 0.1M glycine for 30 minutes to block residual aldehyde group. Sections were washed by 1XPBS 10 minutes three times and permeabilized in ice-clod methanol for 7 minutes, then 1X PBS washed for 10 minutes 2 times. Next, sections were blocked in blocking buffer containing 0.2% Triton-X-100 and 2% BSA in PBS for 1 hour at room temperature, following by incubating with anti-neurofilament (anti-NF, ab8135, rabbit-monoclonal, Abcam, 1:500) and anti-synaptophysin (anti-SYN, ab32127, rabbit-monoclonal, Abcam, 1:250 dilution) in blocking buffer at 4°C overnight. After 1X PBS washing, the sections were incubated with secondary antibodies (488-conjugated goat anti-rabbit, 1:10000 dilution) and Alexa-594-conjugated α-bungarotoxin (α-BTX, B13423, Life technologies, 1:10000 dilution) for 2 hours in dark at room temperature. Last, sections were washed by 1X PBS 10 minutes for 3 times, then mounted with DAPI Fluoromount-G. The immunofluorescence images were visualized and pictured by Carl Zeiss LSM880 confocal microscope and Zeiss Zen black software (confocal pinhole 1.0 Airy unit; collect a z-stack of endplates with a 0.7-1.2μm interval between each optical slice). A-BTX-stained structure that extend < 15μm in the z-dimension is considered as endplate and is imaged for analysis. The intact region of α-BTX, anti-NF and anti-SYN was defined as innervated endplate; while α-BTX only considered as axonal denervation.

doi:10.6342/NTU201902676

2.11 Immunofluorescence assay of spinal cord

The frozen sections of spinal cord were rinsed by 1X PBS for 10 minutes to remove O.C.T. and fixed in 2% PFA for 5=10 minutes. Sections were washed by 1X PBS for 10 minutes 3 times and permeabilized by 1% Triton X-100 in PBS for 3 minutes, then washed by 1X PBS for 10 minutes 3 times immediately. Next, sections were blocked by 5% BSA in PBS for 1.5 hours at room temperature, then incubated with anti-NeuN (MABN140, Millipore, 1:500 dilution) and anti-ChAT (AB144P, Millipore, 1:250 dilution) at 4°C overnight. After reaction with primary antibodies, sections were washed by 1X PBS for 10 minutes 3 times, then incubated with secondary antibodies (Cy3-conjugated goat anti-rabbit and 488-conjugated goat anti-goat, 1:10000 dilution, Jackson ImmunoResearch Laboratories) for 1 hour in dark at room temperature. Finally, sections were washed by 1X PBS for 10 minutes 3 times then mounted with DAPI Fluoromount-G. The immunofluorescence images were visualized and pictured by Zeiss Axioskop 40 Optical Microscope with AxioCam 702 camera and Zeiss Zen blue software. Ventral horn cells with NeuN and ChAT double positive signal with cross-section area (CSA) > 500μm^2 were defined as α-motor neurons.

2.12 Statistical analysis

doi:10.6342/NTU201902676

All statistical analyses and graphs were performed using GraphPad Prism software (GraphPad software Inc.). Results were analyzed by two-tailed student's t test in this study. Data were presented as mean ± standard error of the mean (SEM). P-value < 0.05 was considered as statistically significant.

doi:10.6342/NTU201902676

Chapter 3 Results

3.1 NRIP is a membrane bound AChR structural protein.

The rapsyn is a component of AChR complex proteins, and is a membrane bounded protein that associated with AChR (Cohen et al., 1972; Sobel et al., 1977). Rapsyn with AChR co-targets to cell membrane in non-muscle cells, indicates rapsyn participates in AChR clustering (Marchand et al., 2002). Besides, rapsyn can bind ACTN2, which is a component for NMJ formation (Dobbins et al., 2008). Together, ACTN2, rapsyn and AChR forms AChR complex at NMJ and regulates AChR clustering and NMJ formation. Like rapsyn, our previous studies demonstrated loss of NRIP in muscle causes NMJ abnormality and motor neuron degeneration (Chen et al., 2018). Moreover, in Szu-Wei Chang and Ssu-Yu Lin thesis unpublished results demonstrated that NRIP could bind to ACTN2 EF-hand through IQ domain. Furthermore, (Yun-Hsing Huang thesis) using gastrocnemius (GAS) muscles from 16-week-old WT mice and found that NRIP co-localized with AChRs, ACTN2 and rapsyn, which were known as AChR complex component. Collectively, NRIP colocalized AChR at cell membrane (Yun-Hsing Huang thesis). Thereof, we raised a hypothesis that NRIP might be one of a AChR complex component. Firstly, to examine whether NRIP is a membrane bound protein. The localization of NRIP in 293T cells after transfection 24 hours by immunofluorescence assay (IFA); the EGFP-NRIP localized in both nucleus and cytoplasm (Fig.1A). To see

doi:10.6342/NTU201902676

whether NRIP is a membrane-bound protein, EGFP-NRIP transfected HEK293T cells were fixed and co-stained with fluorescently tagged Wheat Germ Agglutinin (WGA) which was used to label cell membrane and Golgi apparatus (Fig.1B,1C); co-stained with anti-calnexin Endoplasmic Reticulum (ER; Fig.1D). Taken together, NRIP co-localized with membrane, Golgi apparatus and ER markers, indicating that NRIP is a membrane-bound protein. Furthermore, in Ya-Ju Han unpublished results found that half amount of NRIP was localized at cell membrane compared to cytoplasm in C2C12 cells, a mouse myoblast cell line. Collectively, NRIP is a membrane bound protein.

Next, to determine whether NRIP is associated with AChR protein complexes, In the biotin-labeled BTX (B-BTX) pull down assay of WT mice GAS muscles protein, NRIP had been pulled down by B-BTX as well as ACTN2 and rapsyn (Supplementary Fig.S2, unpublished data from Hsin-Hsiung Chen). In sum, NRIP is a membrane bound AChR complex protein.

3.2 NRIP interacts with AChR α subunit through NRIP-C-WD7 domain.

AChR consists of four subunits: α, β, γ and δ. They assembles into $\alpha_2\beta\gamma\delta$ at ER and localizes on postsynaptic muscle membrane (Unwin, 2013). AChR has been reported to have direct binding to rapsyn and ACTN2, which are components of AChR complex (Dobbins et al., 2008; Lee et al., 2009). Based on Supplemental Figure 1, NRIP was a

doi:10.6342/NTU201902676

structural component in AChR complex. We would like to know how NRIP interacts with AChR. To investigate which AChR subunit could bind to NRIP, HEK293T cells were co-transfected with expression vectors for EGFP-tagged NRIP with Flag-tagged AChR-α, or AChR-β or AChR-δ for 48 hours. The cell lysates were harvested and purified by immunoprecipitation (IP) with anti-EGFP antibody (NRIP). Western blot using anti-FLAG revealed the amount of AChR subunits binding with NRIP (Fig. 2A and 2B), the data showed NRIP could interact with AChR-α, β and δ subunits, while AChR-δ have lower binding ability compared with AChR-α. This indicates that NRIP can bind to AChR subunits.

Next, we wanted to discuss which domain of NRIP is responsible for AChR binding. AChR is composed of 4 subunits, NRIP could bind to each subunit of AChR (Fig.2.). We used AChR-α only, a subunit that binds well with NRIP , for investigation of binding mechanism between NRIP and AChR. To make sure whether AChR-α can represent AChR 4 subunits, we compared AChR distribution of co-transfected NRIP and AChR-α or AChR-4 subunits in HEK293T cells after 48 hours. 48 hours transfected 293T cells were stained by anti-EGFP and anti-Flag, that were used to label NRIP and AChR subunits separately (Fig.3). In immunofluorescence assay data of transfecting NRIP and AChR four subunits, we could observe AChR clusters (red) existence and co-localize with NRIP (green) in 293T cells. In 293T cells co-transfected with NRIP and AChR-α, there

doi:10.6342/NTU201902676

was a similar pattern of AChR cluster formation and co-localization with NRIP (Fig. 5A, EGFP and NRIP-FL lane). Based on this result, we would focus on AChR-α for mechanism study to investigate which NRIP domain is responsible for AChR-α binding. We constructed several NRIP mutants previously (Chang et al., 2011), including EGFP-tagged NRIP full length (NRIP-FL); EGFP-tagged N-terminal of NRIP, containing WD1 ~ WD5 (NRIP-N); EGFP-tagged C-terminal of NRIP, containing IQ domain and WD6~WD7 (NRIP-C); EGFP-tagged NRIP full length truncated IQ domain (NRIP-ΔIQ); EGFP-tagged NRIP C-terminal truncated WD7 domain (C-ΔWD7), containing IQ domain and WD6 domain; and EGFP-tagged C-terminal truncated WD6,7 domain (C-ΔWD67), containing IQ domain only (Fig.4A). In Hsin-Hsiung Chen unpublished data, to map which domain could bind to AChR-α, 293T cells were transfected with FLAG-tagged AChR-α and EGFP-tagged NRIP mutants for 48 hours. AChR-α were purified by immunoprecipitation with anti-EGFP antibody and the amount of AChR-α binding with NRIP mutants were showed by western blot using anti-FLAG antibody (Supplementary Fig.S3). The result revealed that NRIP-N had weak AChR-α binding compared to NRIP-FL and NRIP-C. Since NRIP-C showed AChR-α binding while NRIP-N didn't, we assumed that domains in NRIP-C might take part in AChR-α binding. Besides, we could see both C-ΔWD7 and C-ΔWD67 lost AChR-α binding ability comparing to NRIP-FL and NRIP-C. Taken together, WD7 domain of NRIP is responsible for AChR-α binding.

doi:10.6342/NTU201902676

To further confirm this, we reciprocally performed immunoprecipitation using anti-FLAG to purified NRIP mutants' proteins, including NRIP-FL, NRIP-C, NRIP-ΔIQ and C-ΔWD7 (Fig.4B). Western blot using anti-EGFP showed both NRIP-FL, NRIP-C and NRIP-ΔIQ could bind with AChR-α, while C-ΔWD7 could not. Taken together, NRIP-C had AChR-α binding ability, when truncated WD7 domain of NRIP-C lost AChR-α binding affinity. In summary, NRIP and AChR-α is reciprocally interaction through WD7 domain.

3.3 NRIP interacting AChR-α is essential for AChR cluster formation.

Rapsyn can interact with AChR subunits directly (Lee et al., 2009). The rapsyn and AChRs are co-transported to membrane through exocytic pathway, and the agrin can increase rapsyn-AChRs interaction that is correlated with cluster formation in C2C12 cells (Marchand et al., 2002; Moransard et al., 2003). This indicates that rapsyn's interaction with AChR is related to its AChR clustering ability at NMJ (Moransard et al., 2003). As shown in Fig. 4B, NRIP interacted with AChR-α through WD7 domain. Then we would like to investigate whether NRIP's binding ability to AChR is associated with AChR cluster formation. 293T cells were co-transfect with mCherry-tagged AChR-α and EGFP-tagged NRIP mutants for 48 hours. Cells were fixed and fluorescence fusion protein distribution were examined through confocal microscopy, green signals represent

doi:10.6342/NTU201902676

EGFP-NRIP mutants and red signals represent mCherry-AChR-α (Fig.5A). The data showed AChR-α (red) was distributed in several clusters in cells when co-transfecting NRIP-FL (green), while co-transfecting GFP showed distribution of dispersed signals mostly focus around cell nucleus. NRIP mutants such as NRIP-ΔIQ and NRIP-C showed similar pattern as NRIP-FL, the cluster formation could be seen in cytoplasm and membrane. NRIP-N group had dispersed signals in cytoplasm similar to control-GFP group; and few AChR clusters were dispersed when co-transfecting C-ΔWD7. To quantified AChR cluster number in cells, clusters were counted as size >0.5μm^2. The number of AChR clusters were counted in NRIP-FL group and the control-EGFP group (47.95 vs. 0.3 per cell, Fig.5B). The cluster number between NRIP-FL group and NRIP-C group had no significant difference (47.95 vs. 46.65); while C-ΔWD7 group had decrease cluster number compared to NRIP-FL (11.55 vs. 46.65, $P<0.0001$). To further compare AChR cluster number in NRIP mutants, the average cluster number of NRIP-FL set as 100%, cluster number of each mutant was calculated to percentage to NRIP-FL (Fig.5C). Here we set 25% of NRIP-FL cluster number as borderline, cluster number more than 25% of NRIP-FL was defined as positive AChR cluster formation, and cluster number less than 25% NRIP-FL was defined as negative AChR cluster formation in contrast. We examined that NRIP-C and NRIP-ΔIQ had AChR cluster formation ability (95.20% and 84.98%), and NRIP-N and C-ΔWD7 didn't (23.25% and 24.09%).

doi:10.6342/NTU201902676

Furthermore, we analyzed the AChR cluster formation which localized on cell membrane (Fig.5D). NRIP-FL group contained cluster formation on cell membrane while control group (EGFP vector only) didn't (19.7 vs. 0 per cell). The cluster number between NRIP-FL and NRIP-C have no significant difference (19.7 vs. 18.45); while C-ΔWD7 have decrease cluster number than NRIP-FL (11.55 vs. 4.6, $P<0.0001$). Collectively, NRIP is able to form cluster with AChR-α in both cytoplasm and membrane in 293T cells, and C-ΔWD7 lost AChR clustering formation; indicating NRIP's binding to AChR-α through WD7 domain is correlated with its AChR clusters formation.

Next, to examine NRIP mutants' subcellular location, we transfected NRIP-FL, NRIP-N, NRIP-C and C-ΔWD7 to 293T cells, then fixed and observed after 24 hours (Fig.6A). NRIP-FL and NRIP-ΔIQ distributed in both cytoplasm and nucleus, while NRIP-C and C-ΔWD7 distributed only in cytoplasm and NRIP-N in nucleus. In combination NRIP-AChR binding biochemistry with NRIP subcellular location and cluster formation with AChR using IFA analysis (Fig.6B); in sum both NRIP and NRIP-ΔIQ, which expressed in cytoplasm and nucleus, had AChR binding ability and cluster formation in 293T cells. NRIP-N, expressed only in nucleus, had weak AChR binding ability; and no significant cluster formation compared to NRIP-FL. Here we suggest that although NRIP-N contains 5 WD domains, without express in cytoplasm, NRIP-N loss its AChR cluster ability; due to AChR only expressed on cytoplasm and membrane

doi:10.6342/NTU201902676

(Fig.5A). NRIP-C containing two WD domains and one IQ domain expressed in cytoplasm, had good AChR binding ability and cluster formation. Although C-ΔWD7 expressed in cytoplasm, same as NRIP-C, it revealed no AChR binding ability and cluster formation; implying WD7 domain played a major role for AChR binding resulted in cluster formation. In conclusion, NRIP's ability of AChR binding is correlated with its cluster formation, also associated with its expression in cytoplasm. WD7 domain of NRIP is responsible for AChR-α binding, and this interaction is essential for AChR cluster formation.

3.4 NRIP WD7 domain is responsible for NMJ formation in cKO mice.

In our previous studies, the muscle-specific NRIP cKO mice show NMJ abnormality with decreased NMJ area and axonal denervation, loss of motor neuron number in spinal cord and motor function defects at adult age (16week) (Chen et al., 2018). AChR complex components, such as rapsyn, can bind to AChR and mediate its cluster formation at NMJ. In rapsyn deficient mice, AChR is failed to cluster and causes death perinatally (Apel et al., 1997). Previous study used rapsyn$^{+/-}$ (heterozygote) mice, which express less rapsyn in muscle than WT mice. Compared to WT mice, rapsyn$^{+/-}$ mice have reduced rapsyn-to-AChR immunofluorescence ratio and AChR cluster area, indicating that AChR clustering is correlated with rapsyn (Brockhausen et al., 2008). Patients of Congenital myasthenic

doi:10.6342/NTU201902676

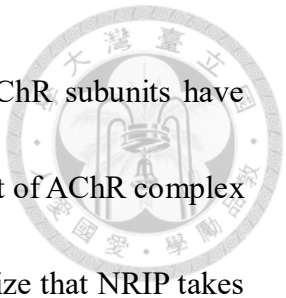

syndromes (CMS) with deficiency of rapsyn but no mutation in AChR subunits have impaired NMJ development (Ohno et al., 2002). NRIP is a component of AChR complex (Fig.2, 4; Supplementary Fig.S2, S4) similar to rapsyn. We hypothesize that NRIP takes part in AChR clustering of NMJ formation. As shown in Fig.6B, NRIP is a structural component of AChR complex, can bind AChR through WD7 domain to form AChR complex cluster in 293T cells. Next, we would investigated whether the the ability of AChR cluster formation in cells can represent NMJ formation in mouse. Here we used muscle-specific NRIP cKO mice to examine NMJ formation by given gene therapy of AAV-NRIP-C and AAV-C-ΔWD7. Previously in Yun-Hsin Huang unpublished data, given intramuscular AAV-NRIP treatment could rescue abnormal phenotypes in NRIP cKO mice, including NMJ area decrease, motor axonal denervation and motor neuron degeneration (Chen et al., 2018). In Fig.5 showed NRIP have AChR cluster formation in cells, and we examined AAV-NRIP treatment have ability to rescue NMJ integrity as well as motor neuron regeneration. As NRIP-C also have AChR cluster formation in cells in Fig.5, we hypothesize that given intramuscular AAV-NRIP-C treatment can rescue abnormal phenotype of NMJ in NRIP cKO mice similar to AAV-NRIP treatment, due to NRIP-C binding with AChR-α. In contrast, given AAV-C-ΔWD7 treatment should be fail to rescue NRIP cKO mice's abnormal phenotype of NMJ; due to lost AChR binding ability. Fig.8A flow chart shows our strategy for examination of NMJ formation in vivo.

doi:10.6342/NTU201902676

Firstly, we generated AAV-NRIP-C and AAV-C-ΔWD7 to perform gene therapy in cKO mice. The adeno-associated viruses (AAV) encoding NRIP-C or C-ΔWD7 were generated by co-transfect pAAV-DJ/8, pHelper and pAAV-MCS-NRIP-C or pAAV-MCS- C-ΔWD7 into HEK293T cells using calcium phosphate transfection for 72 hours. After purification of AAV virus, it was tested by infecting 293T cells for 24 hours in different dosage (For AAV-NRIP-C: 1μl : $1.35*10^8$vg; 5μl : $6.75*10^8$vg; 10μl : $1.35*10^9$vg; 20μl : $2.7*10^9$vg; 50μl : $6.75*10^9$vg; 100μl : $1.35*10^{10}$vg. For AAV- C-ΔWD7: 1μl : $1.78*10^9$vg; 5μl : $8.9*10^9$vg; 10μl : $1.78*10^{10}$vg; 20μl : $3.56*10^{10}$vg; 50μl : $8.9*10^{10}$vg; 100μl : $1.78*10^{11}$vg.) (Fig.7A). Western blot data showed protein expression of NRIP-C and C-ΔWD7 were first seen when given 20 μl virus (AAV-NRIP-C: $2.7*10^9$vg ; AAV- C-ΔWD7: $3.56*10^{10}$vg)for infection, then have increased expression of NRIP-C and C-ΔWD7 when given higher dose (For AAV-NRIP-C, 50μl : $6.75*10^9$vg; 100μl : $1.35*10^{10}$vg. For AAV- C-ΔWD7: 50μl : $8.9*10^{10}$vg; 100μl : $1.78*10^{11}$vg.) of virus for infection. To examine the encoded gene expression in muscle, the IFA data of frozen section from gastrocnemius (GAS) in AAV-NRIP-C ($2.7*10^9$ vg in a total volume of 20 μl for each muscle) and AAV-C-ΔWD7 ($3.6*10^{10}$ vg in a total volume of 20 μl for each muscle) treated cKO mice 1 week after I.M. injection show NRIP-C (green) and C-ΔWD7 (green) expression using anti-EGFP (Fig.7B, middle figure: AAV-NRIP-C treated mice; right figure: AAV-C-ΔWD7 treated mice). To measure whether AAV-NRIP-C or AAV-C-

doi:10.6342/NTU201902676

ΔWD7 gene therapy in NRIP cKO mice can improve NMJ formation and motor neuron deficits, we performed intramuscular (i.m.) injection of AAV-EGFP (control,from Yun-Hsin Huang) ($2*10^{10}$ vg in a total volume of 10 μl for bi-lateral gastrocnemius(GAS) and tibialis anterior muscles), AAV-NRIP-C ($2.7*10^{9}$ vg in a total volume of 20 μl for each muscle) or AAV-C-ΔWD7 ($3.6*10^{10}$ vg in a total volume of 20 μl for each muscle) into bilateral GAS and tibialis anterior muscles at age 6-week old cKO mice. After 10 weeks of virus injection, the mice were scarified and analyzed NMJ integrity and α-motor neuron number (Fig.8A).

To investigate the efficiency of AAV-NRIP-C and AAV- C-ΔWD7 gene therapy in NMJ formation, frozen sections of GAS muscle were cut into 30-μm-thick slices and stained by fluorescence tagged α-BTX, anti-synaptophysin (SYN) antibody and anti-neurofilament (NF) antibody to label AChR, nerve terminals and motor axons at NMJ. Signals of NF and SYN (green) represent axon terminals of motor neurons, while AChR clusters (red) are structures of NMJ (Chen et al., 2018; Tse et al., 2014). Images were captured using confocal microscopy Carl Zesis LSM880 and analyzed by ImageJ software. The NMJ area of AAV-NRIP-C-treated cKO mice was significantly larger than control-treated group (236.06μm^2 vs. 189.05μm^2, $P<0.01$), while AAV-C-ΔWD7 treated group doesn't show significantly larger area than control group (204.31μm^2 vs. 189.05μm^2, Fig.8B, C). The NMJ area of AAV-NRIP-C-treated cKO mice was also

doi:10.6342/NTU201902676

significantly larger than AAV-C-ΔWD7 treated group (236.06μm^2 vs. 204.31μm^2, P<0.05). The overlap of AChRs (red) and axonl terminal (green) was defined as innervation, AChRs only was considered as denervation in contrast. The proportion of denervated endplates decreased in AAV-NRIP-C-treated cKO mice compared with control-treated mice (6.58% vs. 11.36%, Fig.8B, D). AAV-C-ΔWD7-treated cKO mice showed slightly decreased of proportion of denervated endplates than control group (10.70% vs. 11.36%, Fig.8B, D). Taken together, AAV-NRIP-C gene therapy can improve NMJ formation and axonl terminal innervation. Furthermore, to examine motor neuron degeneration in AAV-NRIP-C and AAV-C-ΔWD7 gene therapy, frozen section of spinal cord of the L3-L5 segment were cut into 30-μm-thick slices and stained by anti-neuronal nuclear protein (NeuN) and anti-choline acetyltransferase (ChAT) antibody. Cells with NeuN and ChAT double-positive immnnoactivity and have cross-sectional area (CSA) larger than 500μm^2 in anterior horn were defined as α-motor neuron, which present as color yellow (Fig.9A) (Chen et al., 2018; Misawa et al., 2012). The quantitative data showed α-motor neuron number of AAV-NRIP-C treated cKO mice were higher than control-treated group (23.33 vs. 17.25, P<0.05, Fig.9). AAV-C-ΔWD7 group does not showed significantly decrease α-motor neuron number than control group (17.63 vs. 17.25). To sum up, NRIP WD7 domain's AChR binding ability is responsible for NMJ formation, as well as motor neuron degeneration.

doi:10.6342/NTU201902676

To compare the efficiency of AAV-NRIP-C and AAV-C-ΔWD7 in NMJ formation to AAV-NRIP, which was previously done by Yun-Hsin. Here we analyzed NMJ area, denervated endplates proportion in GAS muscles, and α-motor neuron number in anterior horn of spinal cord by normalizing AAV-NRIP mutants data to AAV-EGFP group's average. The data were then combined and shown in folds of AAV-EGFP group (Fig.10.) For NMJ area, The NMJ area of AAV-NRIP treated cKO mice was larger than control group (1 vs. 1.14, $P<0.05$). The NMJ area of AAV-NRIP-C-treated cKO mice was also larger than control group (1 vs. 1.25, $P<0.001$). There was no significant difference between AAV-C-ΔWD7 treated group and control group (1 vs. 1.08) (Fig.10A). Collectively, AAV-NRIP and AAV-NRIP-C gene therapy in NRIP cKO could rescue NMJ area, but not AAV-C-ΔWD7. In the proportion of denervated endplates, AAV-NRIP treated cKO mice have decreased denervated endplates compare to the control group (1 vs. 0.5, $P<0.001$). There are also decreased of denervated endplates in AAV-NRIP-C-treated cKO mice compared with control mice (1 vs. 0.58, $P<0.05$). In contrast, AAV-C-ΔWD7 treated cKO mice didn't have significantly decreased denervated endplates than control group (1 vs. 0.94) (Fig.10B). Collectively, AAV-NRIP and AAV-NRIP-C gene therapy in NRIP cKO could rescue denervated endplates, but not AAV-C-ΔWD7. For α-motor neuron number in anterior horn of spinal cord, the number of α-motor neuron of AAV-NRIP treated cKO mice were higher than control group (1 vs. 1.17, $P<0.05$). AAV-

doi:10.6342/NTU201902676

NRIP-C treated cKO mice also have more α-motor neuron than control group (1 vs. 1.35, P<0.01). There was no significant difference between AAV-C-ΔWD7 treated group and control group (1 vs. 1.02) (Fig.10C). Collectively, these data showed both AAV-NRIP and AAV-NRIP-C could rescue motor neuron number but not AAV-C-ΔWD7. In sum, AAV-NRIP and AAV-NRIP-C can restore NMJ integrity and motor neuron degeneration, while AAV- C-ΔWD7 group can not. This reveals that NRIP's WD7 domain plays a key role in NRIP's ability for NMJ formation and motor neuron degeneration.

doi:10.6342/NTU201902676

Chapter 4 Discussion

In this study, NRIP localized in membrane, nucleus and cytoplasm, including in ER, Golgi apparatus, and cell membrane of HEK293T cells (Fig.1). In Ya-Ju Han's thesis also showed NRIP localized on C2C12's cell membrane. Hence, NRIP is a membrane bound protein. Besides, Yun-Hsin's thesis demonstrated that NRIP colocalized AChR, rapsyn and ACTN2 on muscle cell membrane. AChR components, such as rapsyn and ACTN2, are known to bind directly or indirectly to AChR and induce AChR clustering (Dobbins et al., 2008; Marchand et al., 2002). Previous study of rapsyn demonstrated that rapsyn localizes at Golgi apparatus, transports with AChR to cell membrane through exocytic pathway. The AChRs presented on COS-7 cell surface are decreased when expressing AChR alone compared to co-expressing rapsyn and AChR. Furthermore, rapsyn colocalizes with AChR in post-Golgi vesicles and cell membrane, indicates that rapsyn can escort AChR to membrane and play a role in stabilization of surface AChRs (Marchand et al., 2000; Marchand et al., 2002). AChR's stability on surface is an equilibrium between rates of insertion and removal of AChRs, and it is regulates by dystrophin-glycoprotein-complex (DGC) (Aittaleb et al., 2017; Bruneau and Akaaboune, 2006). The number/density of AChRs at NMJ is decreased in mice with deficient DGC proteins, such as α-syntrophin, utrophin and α-dystrobrevin (Adams et al., 2000; Martinez-Pena y Valenzuela et al., 2011; Pawlikowski and Maimone, 2009). Rapsyn has

doi:10.6342/NTU201902676

interaction with DGC proteins, α-syntrophin and α-dystrobrevin, that is mediated by utrophin and maintain AChRs' stability (Aittaleb et al., 2017). On the contrast, recent study provides evidence that AChR is responsible for rapsyn's targeting to membrane, while AChR can locate on membrane in rapsyn deficient C2C12 (Chen et al., 2016). As shown on Figure 1, NRIP located in ER, Golgi apparatus and cell membrane, and colocalized with AChR components on cell membrane (Yun Hsin thesis). When NRIP overexpression in C2C12 cells, the cluster formation was enhanced compared with control vector only (Fig. 5B); suggesting that NRIP may involve in cluster formation and be able to escort AChR to cell membrane (Fig.5D). Collectively, NRIP is a membrane-bound protein and colocalizes with AChR complexes in cytosol and cell surface, which is similar to rapsyn.

In this study, we found NRIP as one of an AChR complex components, and participates in AChR clusters formation and neuromuscular junction formation. Previously, in Szu-Wei Chang and Ssu-Yu Lin thesis unpublished results demonstrated that NRIP could directly bind to ACTN2 EF-hand through IQ domain. Here, we demonstrated that NRIP could bind with AChR complexes including rapsyn, ACTN2 by BTX (a neurotoxic protein that binds to AChR) pull down assay both in C2C12 cells and mouse gastrocnemius muscles (unpublished Hsin-Hsiung Chen's data, supplementary Fig.2). The rapsyn, AChR and ACTN2 forms AChR complex at postsynaptic muscle

doi:10.6342/NTU201902676

membrane (Wu et al., 2010). Rapsyn, as a AChR complex component, can bind directly to AChR. Rapsyn is the earliest identified AChR-binding protein, which is found by large-scale purification of membrane fragment in AChR in Torpedo at 1970s (Cohen et al., 1972; Sobel et al., 1977). Rapsyn was then been further studied to induce AChR clustering while co-transfection into non-muscle cells, such as QT-6, COS7, and HEK293T cells, and loss its AChR clustering ability when coiled-coil domain of rapsyn are truncated (Phillips et al., 1991; Ramarao and Cohen, 1998; Yu and Hall, 1994). ACTN2 can bind to rapsyn directly, and associates with AChR clustering at NMJ (Dobbins et al., 2008). Adenomatous polyposis coli (APC), a tumor suppressor protein, can bind specific to β subunit intracellular loop directly (Wang et al., 2003; Wu et al., 2010). APC mainly localizes in cytoplasm and nucleus in the absence of agrin, while co-aggregates with AChR on C2C12 cell membrane when given neural agrin. Besides, the interaction of APC and AChR β loop is required for agrin induced AChR clustering on C2C12 surface (Wang et al., 2003). As a Wnt signaling molecule, APC may also regulate stability of β-catenin, which regulates AChR clustering via binding with rapsyn and α-catenin (Wu et al., 2010; Zhang et al., 2007). Taken together, NRIP can interact with AChR complex components, implying that NRIP is a novel structural component of AChR complex.

Here, we illustrated that NRIP could interact with AChR four subunits and the WD40 domain of NRIP is responsible for AChR α binding. NRIP could bind each subunit, while

doi:10.6342/NTU201902676

AChR-δ revealed lower binding ability compared with AChR-α (Fig. 2). AChR is compose of α, β, γ and δ subunits, they assemble into $\alpha_2\beta\gamma\delta$ in endoplasmic reticulum (ER) membrane and transport to cell membrane through exocytic pathway (γ is replace to ε in adult human) (Marchand et al., 2002; Wanamaker et al., 2003). For AChR binding, rapsyn is known to anchor AChR α, β and ε subunit's α helical domain of intracellular loop, while β subunit shows highest clustering and binding ability to rapsyn (Lee et al., 2009). In this study, we demonstrated that NRIP can bind directly to AChR α, β and δ subunits, while δ subunit showed lower binding ability than other subunits (Fig.2). Four subunits of AChR are individual gene products, but share some common structure: extracellular large NH2-terminal domain; four conserved transmembrane (TM) domain; one cytoplasmic loop with variable size and amino acid sequence and a extracellular COOH-terminal sequence (Albuquerque et al., 2009; Unwin, 2013)(supplementary Fig.1). The largest intracellular domain that locates between TM3 and TM4 is composed of a mix of α-helical and β-strand structure (Albuquerque et al., 2009; Unwin, 2005). The variety of intracellular domain of AChR subunits contributes to different protein-protein interaction, including AChR assembly, subcellular localization and stability (Albuquerque et al., 2009; Kracun et al., 2008). In studies of rapsyn's binding with AChR subunits, rapsyn interacts with subunits' intracellular loops with different affinities (Lee et al., 2009). The intracellular loop amino acid sequences of 4 subunits showed little

doi:10.6342/NTU201902676

similarity, which form various α-helices on intracellular loop. For AChR α, β subunits, there are α-helices of ~40 amino acid each on intracellular loop, while δ subunit loop is predicted to contain shorter α-helix (Le Novere et al., 1999; Lee et al., 2009). The best binding of rapsyn to AChR is thourgh α-helical domain of β subunit's intracellular loop, and δ subunit loop with shorter α-helix is unable to bind with rapsyn (Lee et al., 2009). For another AChR binding protein APC, it only binds to AChR β subunit, indicating the variety of interaction protein between four subunits (Wang et al., 2003). This may explain why NRIP showed different binding ability to AChR subunits, due to the difference of intracellular loop. Besides rapsyn, Lrp4 and MusK are colocalized with AChR on postsynaptic muscle membrane (Valenzuela et al., 1995; Wu et al., 2010). Mice lacking MusK have evenly distributed AChRs and died at birth due to failure of neuromuscular synapse, indicating its importance in NMJ formation (Burden et al., 2018; Lin et al., 2001; Valenzuela et al., 1995). Phosphorylation of Musk by agrin interacts with various protein, such as Dok-7, Dvl and rapsyn, which participate in MusK activation, AChR clustering and scaffolding (Wu et al., 2010). MuSK and rapsyn can co-cluster in QT-6 cells through its binding to rapsyn via the fourth immunoglobulin-like domain. The fourth immunoglobulin-like domain is also associated with AChR clustering on myotubes, suggesting that the domain required for rapsyn's binding of MuSK in QT-6 cells is also required for rapsyn-AChR clustering in myotubes (Zhou et al., 1999). In this study, we

doi:10.6342/NTU201902676

add NRIP as one novel AChR-binding protein.

Further we found that NRIP could bind with AChR-α through WD7 domain on C terminal (Fig.4, supplementary Fig.S3) using immunoprecipitation of NRIP mutants and AChR α subunit. NRIP contains seven WD40 domain and one IQ motifs (Chang et al., 2011; Tsai et al., 2005). IQ motif had been reported to bind to calmodulin (CaM) or EF-hand protein (such as ACTN2) (Bhattacharya et al., 2004). WD40 domain is a 40-66 residue sequence units typically contain WD40 dipeptide at C-terminal, is folded into β-propeller architecture in protein (Xu and Min, 2011). WD40 domain has low level of sequence conservation and a diversity of function, tens of WD40 structure are determined so far. WD40 domain proteins are known to function as protein-protein or protein-DNA platform, interacts with various proteins, peptides and nuclei acid (Stirnimann et al., 2010; Xu and Min, 2011). Like rapsyn, NRIP ‘s binding to AChR through WD7 domain may correlate AChR clustering ability. Similiarly, Coronin 6, a muscle-specific Coronin family member, contains 5 WD40 domain on N-terminal and one coiled-coil domain on C-terminal. Coronin 6 is known to regulates AChR clustering and stabilization by modulating actin cytoskeletal anchorage of AChRs via coiled-coil domain. Although the interaction of Coronin 6 with other AChR components remains unclear, The WD40 domain of Coronin 6 acts as platform for multiple protein interaction, such as rapsyn, and involve in AChR clustering (Chen et al., 2014). This raises a possibility that WD40

doi:10.6342/NTU201902676

repeats' function as protein-protein interaction adapter is important for protein binding to AChRs.

Here, we demonstrated that NRIP's binding to AChR-α was correlated with AChR cluster formation in 293T cells. Similarly, the rapsyn's coiled-coil domain is responsible for AChR binding and clustering in 293T cells (Ramarao et al., 2001). Furthermore, in C2C12 cells, agrin increases rapsyn's interaction with surface AChR, and the increased rapsyn-AChR interaction correlates with more AChR clustering on cell membrane (Moransard et al., 2003). This reveals that AChR's binding is associate with AChR clustering formation in cells. Our results revealed the binding and cluster formation between AChR α subunit and NRIP mutants in 293T cells (Fig.5-6); NRIP-FL, NRIP-ΔIQ and NRIP-C, which showed binding affinity to AChR α subunit in biochemistry assay, could induce AChR cluster formation in 293T cells. C-ΔWD7 lost AChR-α binding ability, therefore had decreased AChR cluster number in 293T cells. This indicates that NRIP's binding to AChR-α correlates with AChR cluster formation in cells. Although NRIP-N showed weak AChR-α binding ability in biochemistry assay coupled with the decreased AChR cluster number similar to C-ΔWD7 group. This may be due to NRIP-N expressed only in nucleus, not in cytoplasm (Fig.6A) resulted in the failure to form AChR clusters.

In this study, we further confirmed NMJ formation between motor neuron axon and

doi:10.6342/NTU201902676

muscle is correlated with the AChR binding resulted in cluster formation in cell lines. During NMJ formation, AChR clustering at postsynaptic membrane through agrin-Lrp4-MuSK signaling pathway. Agrin that released from presynaptic motor neuron would phosphorylate MuSK through Lrp4, further triggers signaling pathways that induce stabilization of AChR clusters, like rapsyn for example (DeChiara et al., 1996; Kim et al., 2008). AChR complex component, such as rapsyn, have ability to bind directly with AChR and participates in AChR cluster formation and stabilization in NMJ (Burden et al., 2018). In previous study, we demonstrated that global NRIP knockout (gKO) mice have impaired motor performance and delayed muscle regeneration (Chen et al., 2015). We further generated muscle specific NRIP knockout (cKO) mice, and examined muscle weakness with abnormal NMJ architecture and axonal denervation at 16 weeks compared with WT (Chen et al., 2018). The abnormal NMJ architecture includes decrease NMJ area and denervation of motor axon terminal at muscle. Besides, there are loss of motor neuron in cKO spinal cord at age 16 weeks (Chen et al., 2018). These indicates that deprivation of NRIP in muscle would affect NMJ formation and stabilization in adult mice. AAV-NRIP-C, which showed AChR binding (Fig. 2) and clustering in cells (Fig. 4), gene therapy in NRIP cKO could increase NMJ area; but AAV-C-ΔWD7, with negative AChR binding (Fig. 2) and clustering in cells (Fig. 4), not effect on restoration of NMJ abnormality of NRIP cKO (Fig.8); hence NMF formation are correlated with AChR

doi:10.6342/NTU201902676

binding and AChR cluster formation. In our study, NRIP is an AChR complex, and its cluster formation in cells is related with NRIP binding with AChR. Furthermore, the binding to AChR through WD7 correlates to AChR cluster formation on postsynaptic muscle membrane in vivo. This further confirm the importance of WD7 domain in NMJ formation, due to its AChR binding ability. Collectively, NRIP interacting AChR can result in cluster formation in cells and NMJ formation in mice.

NMJ formation is important for muscle contraction. During innervation of NMJ, agrin induces phosphorylation of AChR β subunit through phosphorylated MuSK, further recruit additional rapsyn binding with AChR. The recruitment of additional rapsyn also gather more AChR that previously binding with rapsyn to cluster together, induce AChR cluster formation on membrane in C2C12 cells. (Borges et al., 2008; Lee et al., 2009). These reveal that rapsyn's binding to AChR is associated with its AChR cluster formation and stabilization on postsynaptic muscle membrane through agrin-Lrp4-MusK signaling pathway (Borges et al., 2008; Brockhausen et al., 2008; Burden et al., 2018). Additionally, rapsyn's E3 ligase activity in AChR clustering, the rapsyn-induced AChR clustering in 293T cells corresponding to rapsyn-induced AChR clustering on C2C12 cell membrane and NMJ formation in mice (Li et al., 2016). In rapsyn+/- (heterozygote) mice, which express less rapsyn in muscle than WT mice, there are decreased AChR aggregation at postsynaptic muscle membrane (Brockhausen et al., 2008).

doi:10.6342/NTU201902676

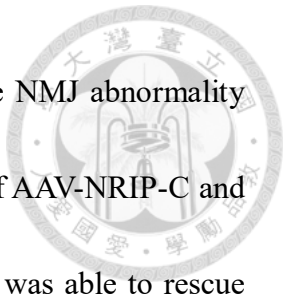

Here, we demonstrated that NRIP-C fragment could rescue the NMJ abnormality and motor neuron survival in NRIP cKO mice. AAV gene therapy of AAV-NRIP-C and AAV-C-ΔWD7 to NRIP cKO mice demonstrated that AAV-NRIP-C was able to rescue NMJ formation and motor neuron degeneration, while AAV-C-ΔWD7 wasn't (Fig.7-9). For patients of Congenital myasthenic syndromes (CMS) with deficiency of NMJ component, like agrin, Lrp4, MusK and rapsyn, have impaired NMJ development (Engel et al., 2015; Ohno et al., 2002). This reveals the importance of AChR-related component in NMJ formation and maintenance. In Yun-Hsin's thesis, gene therapy of intramuscular injection of AAV-NRIP can rescue NMJ integrity and motor neuron degeneration in cKO mice. In this study, we compared the efficiency of AAV-NRIP-C and AAV- C-ΔWD7 gene therapy in NMJ formation. AAV-NRIP-C treatment could rescue NMJ area and denervation of motor axon terminal, while AAV-C-ΔWD7 treatment could not. For motor neuron degeneration, AAV-NRIP-C treatment prevented motor neuron death in cKO spinal cord, AAV-C-ΔWD7 did not in contrast. Taken together, AAV-NRIP-C have ability to improve NMJ formation and maintenance of cKO mice at age 16 weeks, but lost it when WD7 domain is truncated. Compare data of AAV-NRIP-C and AAV-C-ΔWD7 to AAV-NRIP, which was done by Yun-Hsin, we could see that AAV-NRIP-C had similar efficiency of rescuing NMJ integrity and motor neuron degeneration (NMJ area: 1 vs. 1.25, $P<0.001$; denervation fold: 1 vs. 0.58, $P<0.05$; α-motor neuron: 1 vs. 1.35, $P<0.01$,

doi:10.6342/NTU201902676

Fig.10). Hence except AAV-NRIP could rescue NMJ formation and motor neuron survival, the AAV-NRIP-C (only containing IQ, WD6 and WD7) had a function for restore NMJ abnormality of NRIP cKO. In the future, AAV-NRIP-C has a potential as a therapeutic drug for the treatment of NMJ impairment, such as ALS, myasthenia gravis (MG) and Congenital myasthenic syndromes (CMS).

As to the role of NRIP on NMJ, NRIP could interact with AChR, ACTN2, and actin (unpublished results); NRIP may act as a scaffolod protein to stablilize NMJ formation. Like the dystrophin glycoprotein complex (DGC) at neuromuscular junction, that compose of α-syntrophin, α-dystrobrevin, dystrophin utrophin and dystroglycan, is important for structure integrity of synapse and muscle (Blake et al., 2002). α-syntrophin and α-dystrobrevin form complex with rapsyn via utrophin in AChR-rich domain, and contribute to AChR stability at NMJ (Aittaleb et al., 2017). On the other hand, microtubule actin cross linking factor1 (MACF1) colocalized with rapsyn and AChR at NMJ, can recruit microtubule network and maintain AChR density at NMJ (Oury et al., 2019). This reveals the importance of AChR related scaffold protein that support AChR stably clustering on cell surface at NMJ.

In conclusion, NRIP is a membrane-bounded AChR complex component. NRIP can bind to AChR-α reciprocally through WD7 domain on C terminal. With WD7 domain's binding ability to AChR, NRIP is able to form AChR clusters in 293T cells. Furthermore,

doi:10.6342/NTU201902676

the cluster formation examined in vitro is related to AChR cluster formation at NMJ in vivo. By AAV gene therapy we can see that AAV-NRIP-C treatment is able to improve NMJ integrity and motor neuron survival in NRIP cKO mice, similar to AAV-NRIP treatment, due to WD7 domain's binding to AChR-α. These demonstrate the importance of NRIP in AChR cluster formation during NMJ formation and maintenance as a novel AChR structural component.

doi:10.6342/NTU201902676

Chapter 5 Figures

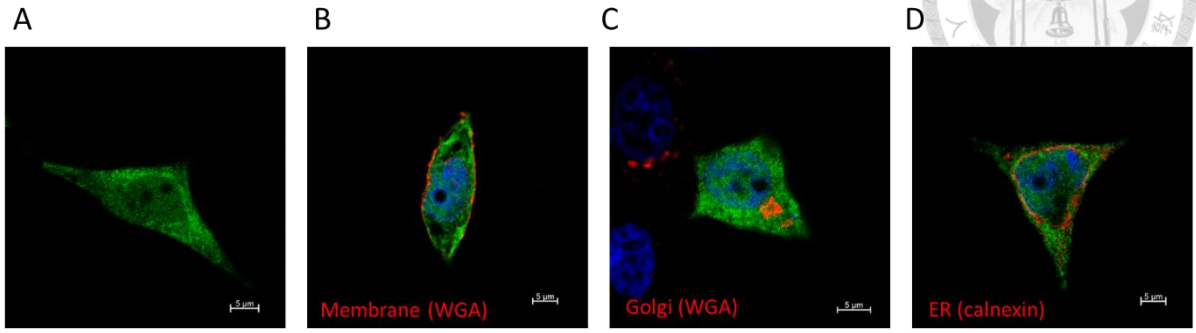

Fig.1. NRIP is a membrane-bound protein.

(A)The plasmid (named nuclear receptor interaction protein (NRIP-EGFP) was transfected into HEK293T cells by jetPRIME. After 24 hours, immunofluorescence assay was performed to examine NRIP distribution. EGFP-NRIP (green) localized at cytosol, membrane, and nucleus. (B) Co-stained with Wheat Germ Agglutinin (WGA; red, for cell membrane) and anti-GFP (NRIP). For WGA immunofluorescence staining of cell membrane, cells were incubated with WGA after 2% paraformaldehyde fixed, before permeabilized. Green: NRIP; red: cell membrane. (C) Co-stained with WGA(red, for Golgi apparatus) and anti-GFP (NRIP). For WGA immunofluorescence staining of Golgi apparatus, cells were incubated with WGA after 2% paraformaldehyde fixed and permeabilized by ice-cold methanol. Green: NRIP, red: Golgi apparatus. (D) Co-stained with calnexin (red, for endoplasmic reticulum marker) and anti-GFP (NRIP). Green: NRIP; red: endoplasmic reticulum (ER). Scale bar, 5μm.

doi:10.6342/NTU201902676

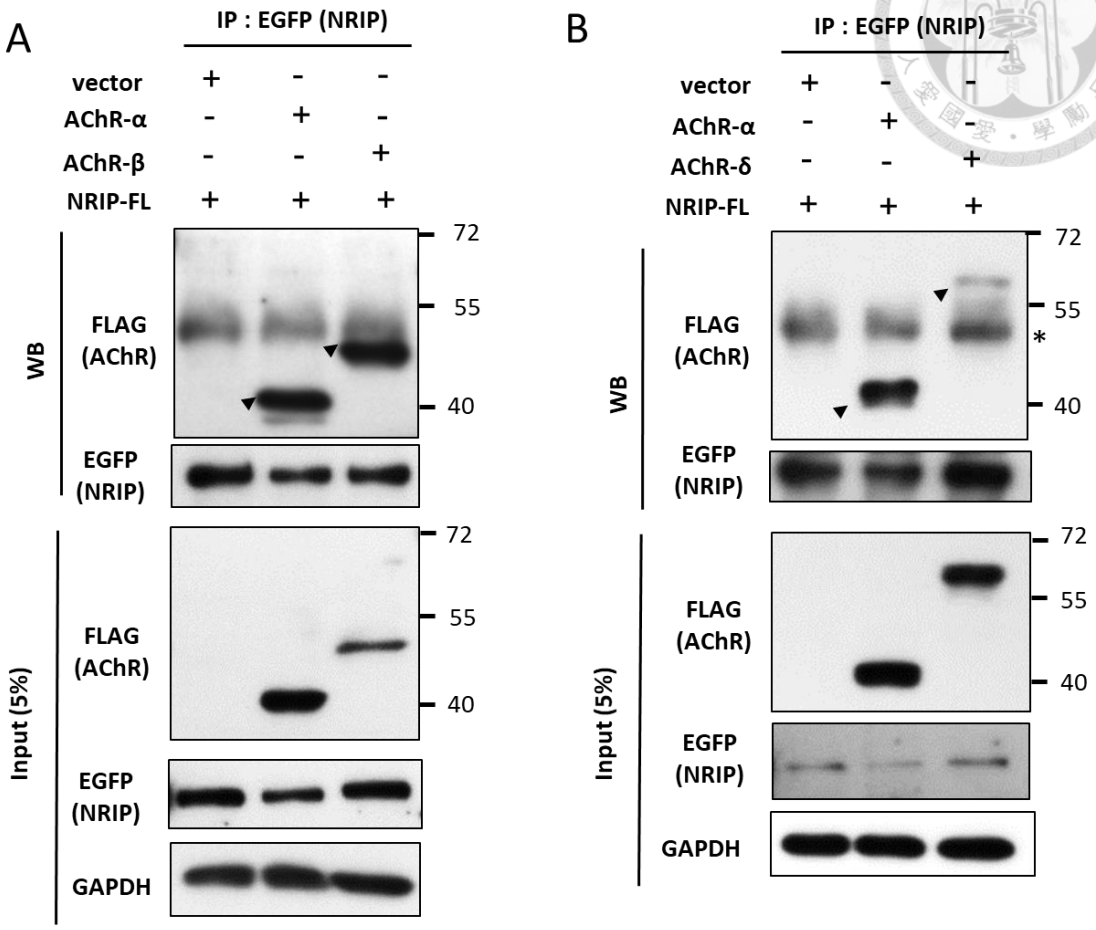

Fig.2. NRIP can interact with AChR α, or β, or δ subunit.

(A) NRIP interacts with either AChR-α or β. HEK293T cells were transfected with EGFP-NRIP and Flag-AChR-α or Flag-AChR-β by jetPRIME. 48 hours after transfection, immunoprecipitation with anti-EGFP (NRIP) was performed from of each transfected lysates; and then western blot analysis by anti-Flag (AChR). Total 1mg lysates were performed immunoprecipitation assay and 50 μg (5% of immunoprecipitation lysates) as input. GAPDH as an internal control. Arrow head indicates the precipitated AChR by NRIP. (B) NRIP interacts with either AChR-α or δ. HEK293T cells were transfected with EGFP-NRIP and Flag-AChR-α or Flag-AChR-β by jetPRIME transfection. Immunoprecipitation with anti-EGFP (NRIP) was performed from each transfected lysates; and then western blot analysis by anti-Flag (AChR). Total 1mg lysates were performed immunoprecipitation assay and 50 μg (5% of immunoprecipitation lysates) as input. GAPDH as an internal control. Arrow head indicates the precipitated AChR by NRIP, while star sign represents heavy chain.

doi:10.6342/NTU201902676

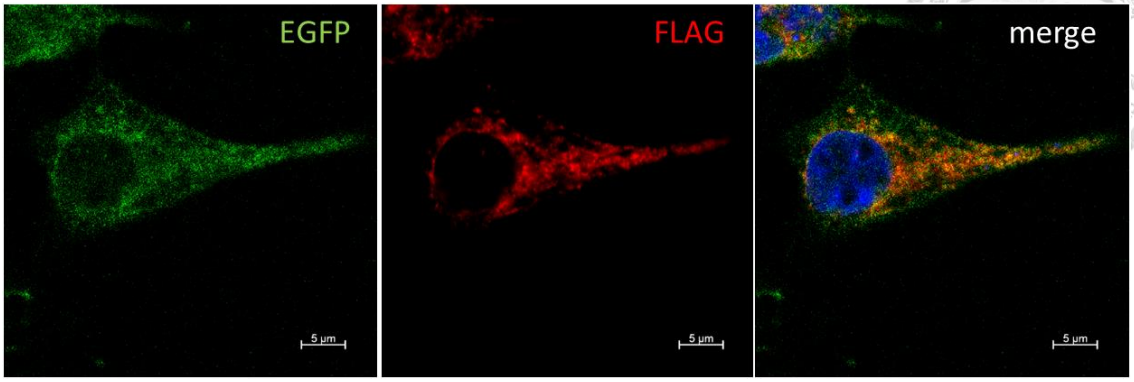

Fig.3. NRIP colocalizes with AChR α, β, γ, δ.

Immunofluorescence assay with anti-GFP (green) and anti-Flag (red) in HEK293T cells co-transfected Flag-AChR α, β, γ, δ subunits together with EGFP-NRIP by jetPRIME for 48 hours. NRIP was colocalized with AChR 4 subunits in cells (merge). The AChR aggregation was counted by area >0.5 μm^2 as AChR cluster). The AChR aggregates in cytoplasm were observed in cytoplasm when co-transfect EGFP-NRIP. Scale bar, 5 μm.

doi:10.6342/NTU201902676

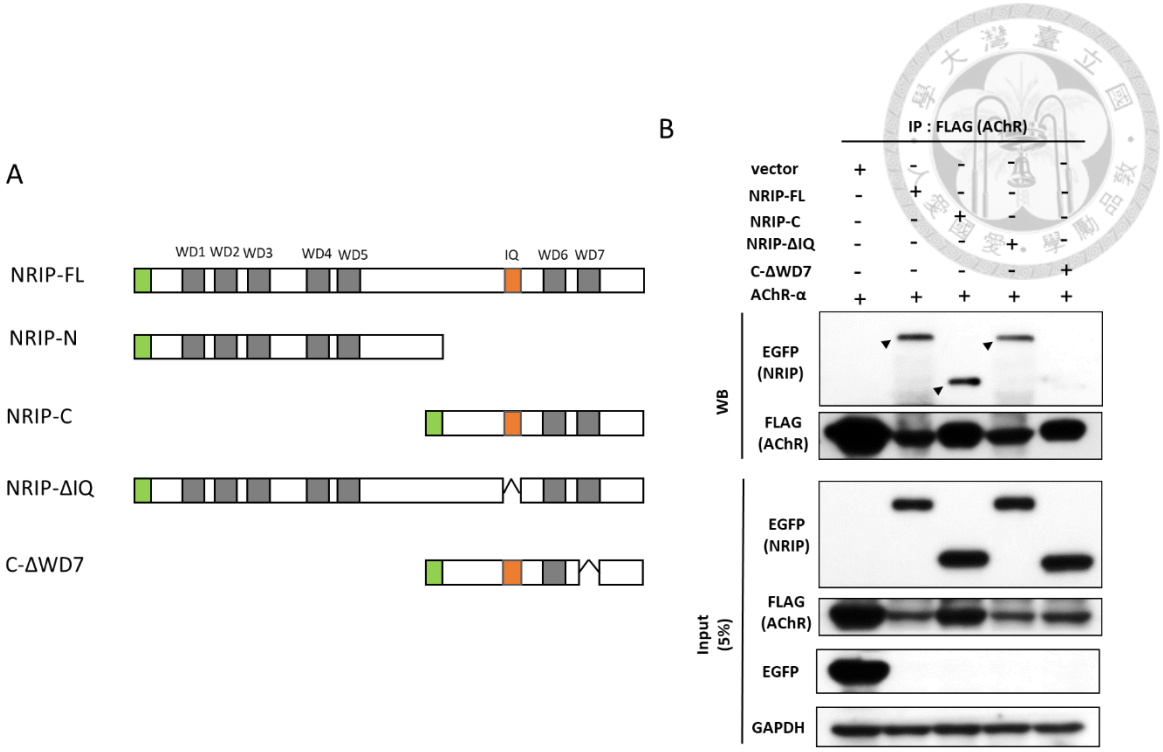

Fig.4. The WD40 domain 7 located at NRIP-C is responsible for for AChR-α binding. (A) Schematic map of NRIP mutants. Green box represents EGFP, grey box as WD40 domains, and orange box as IQ domain. The mutants include: EGFP-tagged NRIP full length (NRIP-FL); EGFP-tagged N-terminal of NRIP, containing WD1 ~ WD5 (NRIP-N); EGFP-tagged C-terminal of NRIP, containing IQ domain and WD6~WD7 (NRIP-C); EGFP-tagged NRIP full length truncated IQ domain (NRIP-ΔIQ), containing WD1 ~ WD7 domain and truncated IQ domain; EGFP-tagged NRIP C-terminal truncated WD7 domain (C-ΔWD7), containing IQ domain and WD6 domain; and EGFP-tagged C-terminal truncated WD6,7 domain (C-ΔWD67), containing IQ domain only (B) Mapping domain of NRIP for AChR-α binding. Immunoprecipitation assay for NRIP mutants-binding with AChR-α, HEK293T cells were transfected with Flag-AChR-α and EGFP-NRIP mutants by jetPRIME for 48 hours. Immunoprecipitation with anti-FLAG (AChR-α) was performed from each transfected lysates; and then western blot analysis by anti-GFP (NRIP). Total 1mg lysates were performed immunoprecipitation assay and 50 μg (5% of immunoprecipitation assay) as input. GAPDH as an internal control. Both NRIP-FL and NRIP-ΔIQ had interaction with AChR-α. EGFP-NRIP-C, containing WD6 and WD7 domain, had AChR binding ability; while C-ΔWD7 lost AChR-α binding; indicating WD7 domain is responsible for AChR-α binding. Arrow head: the precipitated NRIP mutant protein by AChR-α.

doi:10.6342/NTU201902676

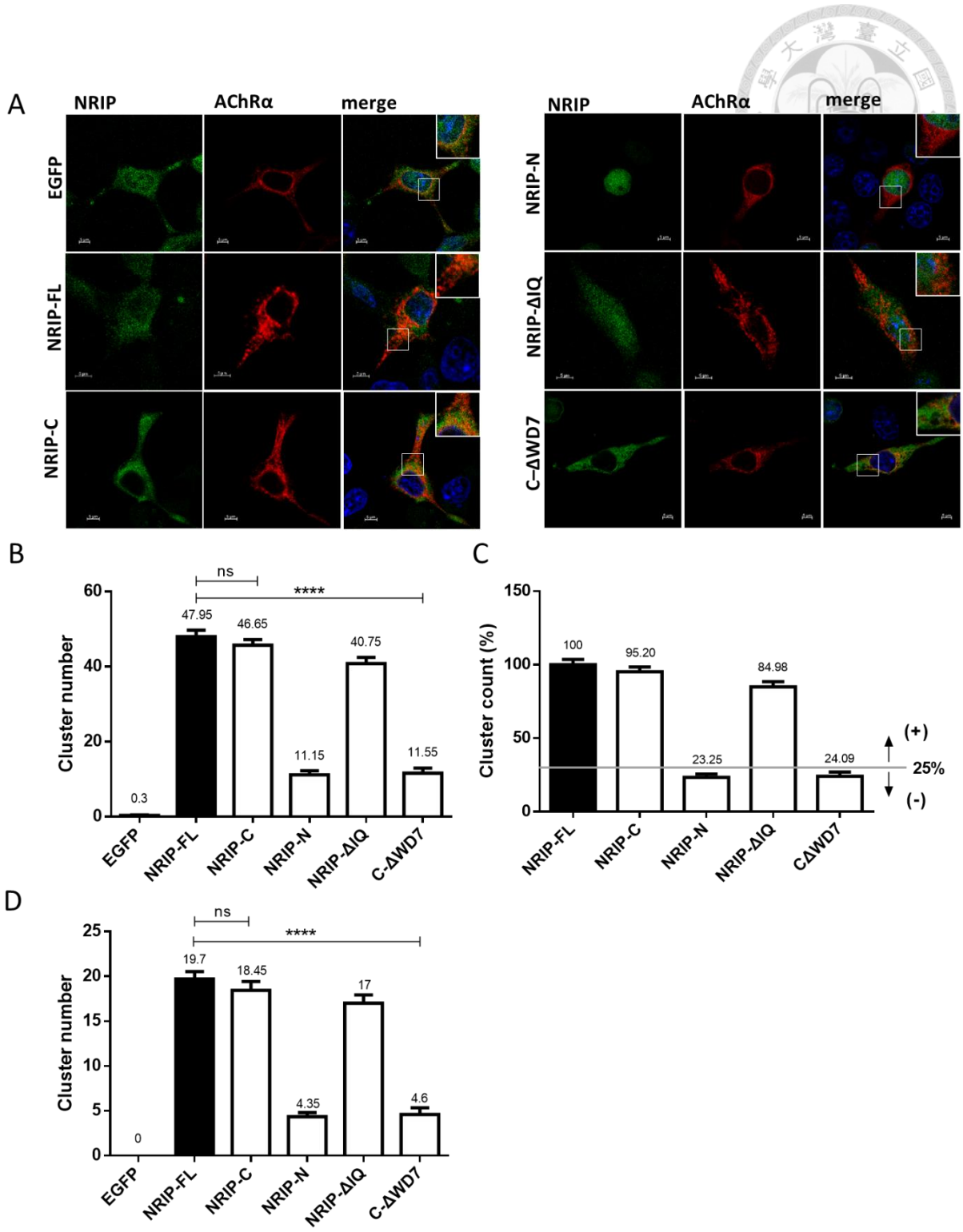

Fig.5. The cluster formation of NRIP with AChR-α in 293T cells.

(A) HEK293T cells were co-transfected with mCherry-AChR-α and each EGFP-NRIP mutant by jetPRIME for 48 hours. The plasmid (pmCherry-AChR-α) was constructed by Hsin-Hsiung Chen (Supplementary Fig.S5.). The cells were fixed and then pictured by confocal microscopy without antibody labeling, that the green and red signals were self-fluorescence of EGFP and mCherry. Green: EGFP or NRIP mutants; red: AChR-α; merge:

doi:10.6342/NTU201902676

combine signals of EGFP-NRIP mutant and AChR-α. The AChR aggregation area >0.5 μm are defined as AChR cluster. Scale bar, 5μm. (B) Quantification analysis of the cluster number was counted as the AChR aggregation size >0.5μm. NRIP-FL group contained more cluster formation than control (EGFP vector only) (47.95 vs. 0.3 per cell). The cluster number between NRIP-FL and NRIP-C have no significant difference (47.95 vs. 46.65); while C-ΔWD7 have decrease cluster number than NRIP-FL (11.55 vs. 46.65, P<0.0001). (C) Quantification analysis of % of NRIP mutants for cluster formation to NRIP-Fl. The average cluster number of NRIP-FL set as 100%, cluster number of each mutant was calculated to percentage to NRIP-FL. Set 25% of NRIP-FL cluster number as border line, cluster number which is more than 25% of NRIP-FL were defined as positive AChR cluster formation, such as NRIP-C and NRIP-ΔIQ (95.20% and 84.98%). Cluster number which is less than 25% NRIP-FL was defined as negative AChR cluster formation, such as NRIP-N and C-ΔWD7 (23.25% and 24.09%). (D) Quantification analysis of the cluster number locolized on cell membrane was counted as the AChR aggregation size >0.5μm. NRIP-FL group contained cluster formation on membrane while control group (EGFP vector only) didn't (19.7 vs. 0 per cell). The cluster number between NRIP-FL and NRIP-C have no significant difference (19.7 vs. 18.45); while C-ΔWD7 have decrease cluster number than NRIP-FL (11.55 vs. 4.6, P<0.0001). Total 20 cells per group were counted from 5 independent experiments. Data are mean ± SEM by two tailed Student's t-test. ****P<0.0001; ns: no significance.

doi:10.6342/NTU201902676

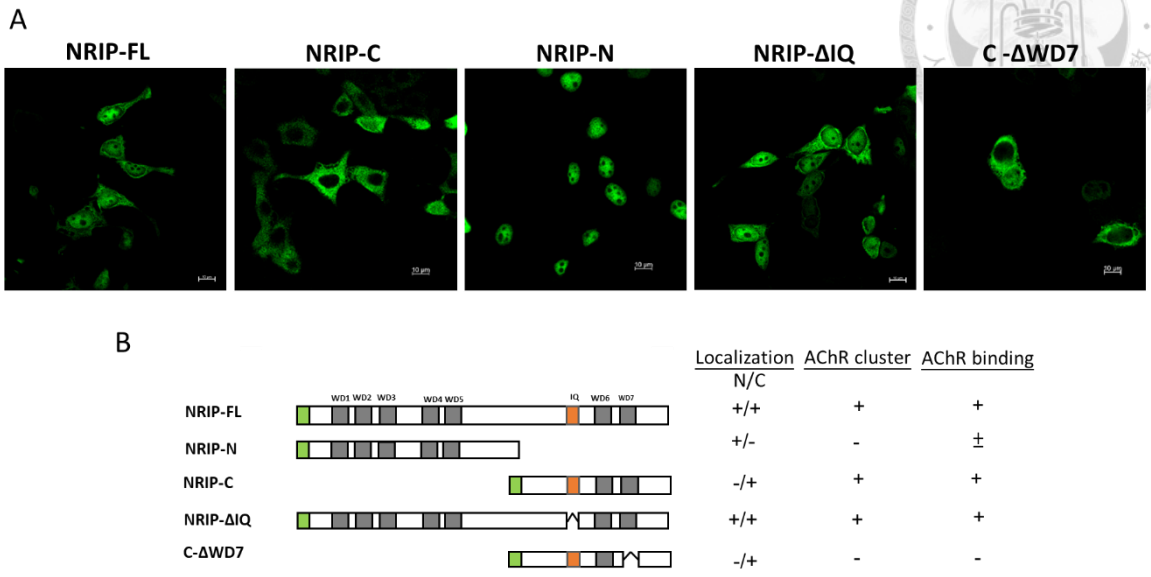

Fig.6. Subcellular location of NRIP mutants in HEK293T cells.

(A) Fluorescent image of EGFP-NRIP (green) subcellular location at HEK293T cells. 24 hours after transfection; NRIP-full length and NRIP-ΔIQ expressed both at cytoplasm and nucleus, while NRIP-C expressed only in cytoplasm, and NRIP-N expressed in nucleus. (B) Summary of the subcellular location, AChR-α binding and cluster formation. Both NRIP and NRIP-ΔIQ, which expressed in cytoplasm and nucleus, had AChR-α binding ability and cluster formation in HEK293T cells. NRIP-N, expressed only in nucleus, had weak AChR binding ability and cluster formation compared to NRIP. NRIP-C, expressed in cytoplasm, had strong AChR binding ability and cluster formation. C-ΔWD7 expressed in cytoplasm same as NRIP-C, but lost its binding ability and cluster formation due to loss of WD7; implying that WD7 domain of NRIP is responsible for AChR-α binding. Scale bar, 10μm.

doi:10.6342/NTU201902676

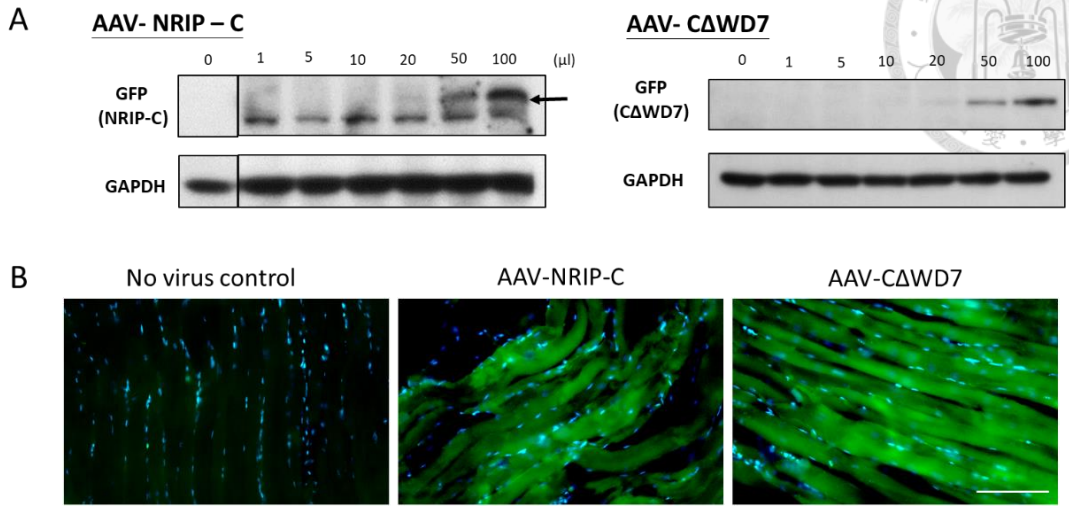

Fig.7. Adeno-associated virus (AAV)-NRIP C and AAV-C-ΔWD7 generation.

The adeno-associated viruses (AAV) encoding NRIP-C or C-ΔWD7 were generated. Co-transfected pAAV-DJ/8, pHelper and pAAV-MCS-NRIP-C (or pAAV-MCS- CΔWD7) into HEK293T cells using calcium phosphate transfection for 72 hours; the cell lysates were harvested and cells were broken by several freeze/thaw cycles. Supernatant viruses were harvested and purified through CsCl density-gradient ultracentrifugation and dialysis. (A) Western blot analysis of the recombinant AAV-NRIP-C and AAV-C-ΔWD7 infection efficiency. The recombinant viruses were infected in HEK293T cells; 24 hours after infection, anti-EGFP was immunostained for NRIP-C and C-ΔWD7 expression in different dose of viruses; due to each construct contained EGFP tag. GAPDH as internal control. Left panel: arrow indicates NRIP-C's band. Right panel: expression of C-ΔWD7 in different dose. (B) Immunofluorescence assay of anti-EGFP (green) for NRIP-C or C-ΔWD7) expression and DAPI (nucleus, blue) in frozen sections from gastrocnemius (GAS) in AAV-treated NRIP cKO mice. 6-weeks cKO mice were given intramuscular injection to bilateral GAS muscles of virus (AAV-NRIP-C: $2.7*10^9$ vg in a total volume of 20 μl for each muscle; AAV- C-ΔWD7: $3.6*10^{10}$ vg in a total volume of 20 μl for each muscle.). GAS muscles were collected 1 week after virus injection. GAS muscles of WT mice without virus infection were collected as no virus control. Scale bar, 50μm.

doi:10.6342/NTU201902676

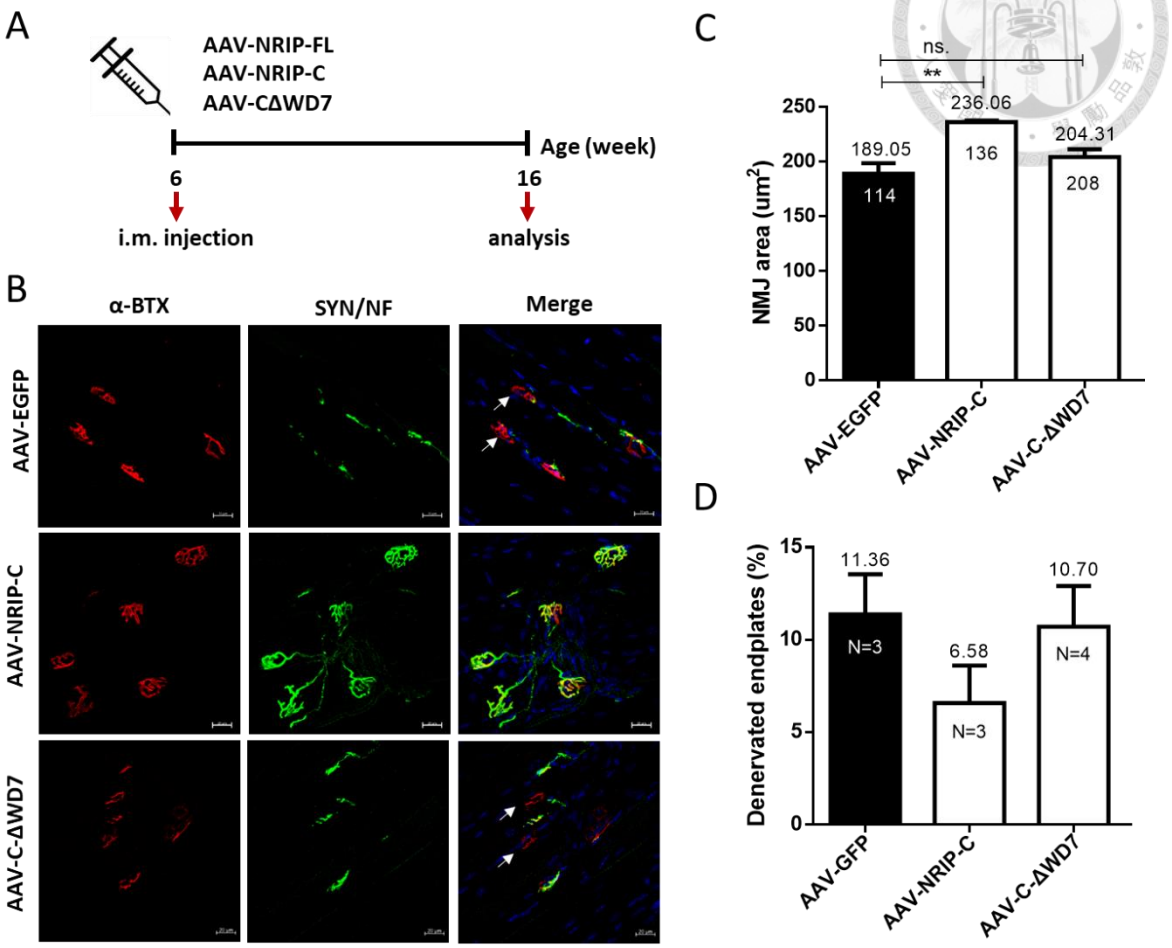

Fig.8. Intramuscular NRIP-C gene therapy of NRIP cKO can rescue neuromuscular integrity.

(A) Schematic protocol for AAV-NRIP-C gene therapy. Given intramuscular (i.m.) injection of AAV-EGFP (control), AAV-NRIP-C or AAV-C-ΔWD7 into bilateral gastrocnemius and tibialis anterior muscles at age 6-week old NRIP cKO mice. 10 weeks after injection, the mice were sacrificed and analyzed NMJ integrity and α-motor neuron number. (B) Immunofluorescence assay of α-BTX [red, for acetylcholine receptors (AChRs)], anti-synaptosphysin (SYN) and anti-neurofiliment (NF) [green, for axonal terminals] and DAPI (blue) in frozen sections from gastrocnemius (GAS) in AAV-treated cKO mice 10 week after virus injection. Scale bar, 20 μm. (C) Quantitative analysis of neuromuscular junction area. The quantification of NMJ area was analyzed by ImageJ software. The NMJ area of AAV-NRIP-C-treated cKO mice was larger than control group (236.06 μm^2 vs. 189.05 μm^2, $P<0.01$) and AAV-C-ΔWD7 treated group (236.06 μm^2 vs. 204.31 μm^2, $P<0.05$). Control, N=3 mice; AAV-NRIP-C treatment, N=3 mice; AAV-C-ΔWD7 treatment, N=4 mice. The number inside each bar represents the number of

doi:10.6342/NTU201902676

examined NMJ (at least 30 NMJs were counted each GAS). (D) Axon denervation analysis. Denervation was defined as no nerve terminal overlapped to AChR cluster. White arrow indicates denervation endplates. The proportion of denervated endplates (measured by the percentage of denervated endplates to the total endplates on one GAS muscle frozen section), decreased in AAV-NRIP-C-treated cKO mice compared with control mice (6.58% vs. 11.36%); compared with AAV-C-ΔWD7 (6.58% vs. 10.70%). Control, N=3 mice; AAV-NRIP-C treatment, N=3 mice; AAV-C-ΔWD7 treatment, N=4 mice. Data are mean ± SEM by two tailed Student's t-test. *P<0.05 and **P<0.01

doi:10.6342/NTU201902676

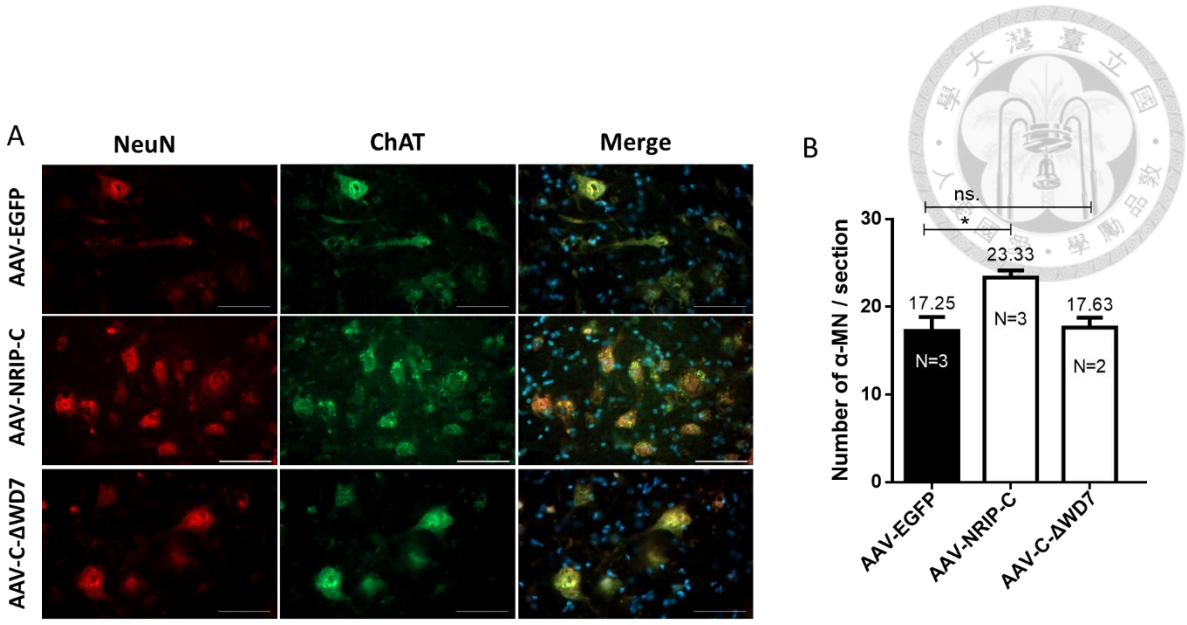

Fig.9. Intramuscular NRIP-C gene therapy can rescue the survival of motor neurons of NRIP cKO mice.

(A) Immunofluorescence assay of NeuN (red), ChAT (green) and DAPI (blue) in frozen section of spinal cord L3-L5 regions from AAV-treated cKO mice was performed 10 weeks after virus injection. Yellow cells which showed double positive signal of NeuN and Chat with cross-section area (CSA) >500 μm^2 would be counted as α-motor neurons. Scale bar, 50 μm. (B) Quantification analysis of α-motor neuron number per anterior horn. The α-motor neuron numbers of AAV-NRIP-C treated cKO mice were higher than control group (23.33 vs. 17.25, P<0.05). AAV-NRIP-C treated cKO mice also had higher α-motor neuron numbers than AAV-C-ΔWD7group (23.33 vs. 17.63, P<0.05). Control, n=3 mice; AAV-NRIP-C treatment, n=2 mice; AAV-C-ΔWD7 treatment, n=3 mice. Data are mean ± SEM by two tailed Student‘s t-test. *P<0.05

doi:10.6342/NTU201902676

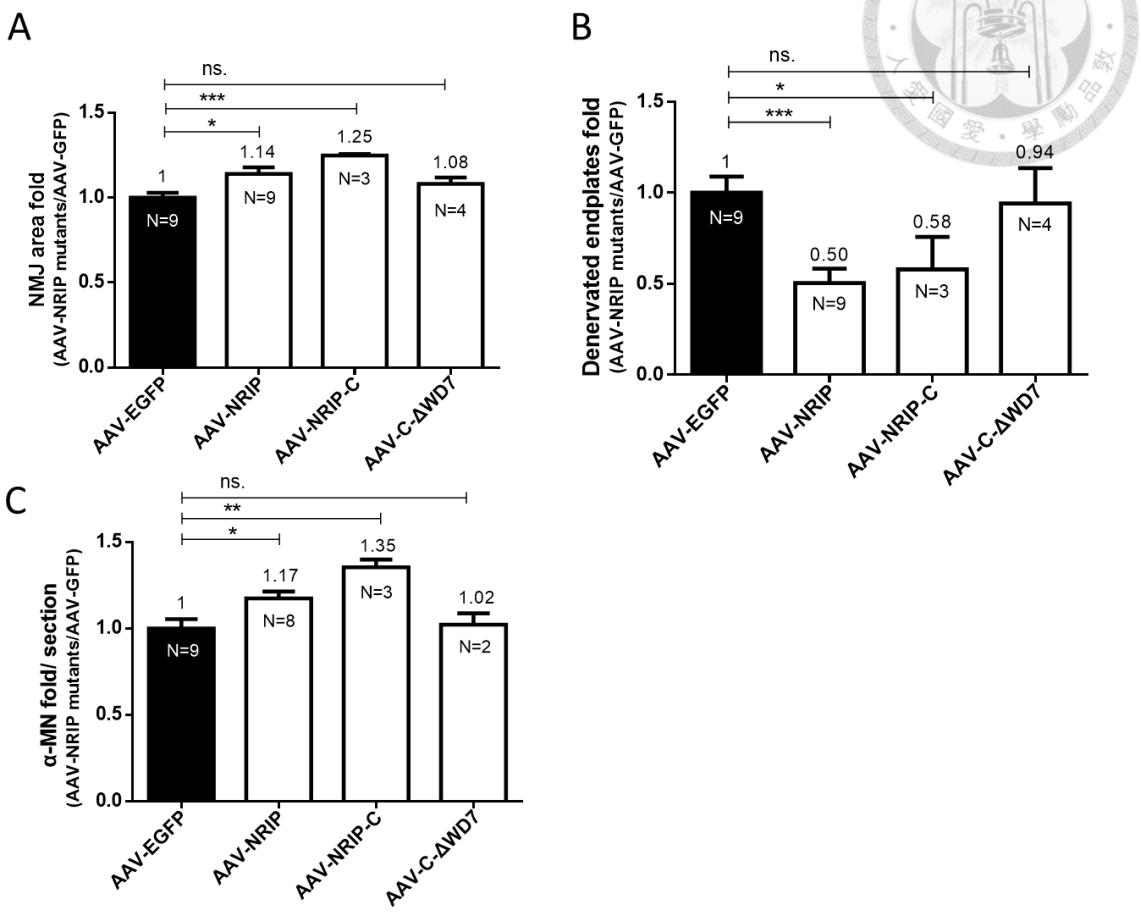

Fig.10. Summary comparison of intramuscular AAV-NRIP mutants gene therapy in rescuing neuromuscular integrity and survival of motor neuron in NRIP cKO mice. These data were in combination with Yun-Hsin' data by normalized AAV-NRIP mutants data to AAV-EGFP group.

(A) Quantitative analysis of neuromuscular junction area. The quantification of NMJ area of NRIP mutants was analyzed, NRIP mutants were normalized to AAV-EGFP group (set as 1), then analyzed as fold change of each mutant to the corresponding AAV-EGFP control. The NMJ area of AAV-NRIP treated cKO mice was larger than control group (AAV-EGFP) (1 vs. 1.14, $P<0.05$). The NMJ area of AAV-NRIP-C-treated cKO mice was also significantly larger than control group (1 vs. 1.25, $P<0.001$). There was no significant difference between AAV-C-ΔWD7 treated group and control group (1 vs. 1.08). Control, N=9 mice; AAV-NRIP treatment, N=9; AAV-NRIP-C treatment, N=3 mice; AAV-C-ΔWD7 treatment, N=4 mice. (B) Axon denervation analysis. The proportion of denervated endplates of NRIP mutants was normalized to AAV-EGFP group, then analyzed as fold change (NRIP mutant/EGFP control). Compare to the control group, AAV-NRIP treated cKO mice had decreased denervated endplates (1 vs. 0.5, $P<0.001$).

doi:10.6342/NTU201902676

The proportion of denervated endplates also decreased in AAV-NRIP-C-treated cKO mice compared with control mice (1 vs. 0.58, P<0.05). In contrast, AAV-C-ΔWD7 treated cKO mice didn't have significantly decreased denervated endplates than control group (1 vs. 0.94). Control, N=9 mice; AAV-NRIP treatment, N=9 mice; AAV-NRIP-C treatment, N=3 mice; AAV-C-ΔWD7 treatment, N=4 mice. (C) Quantification analysis of α-motor neuron number per anterior horn. The α-motor neuron numbers were normalized to AAV-EGFP group, then analyzed as fold change. The number of α-motor neuron of AAV-NRIP treated cKO mice were higher than AAV-EGFP-control group (1 vs. 1.17, P<0.05). AAV-NRIP-C treated cKO mice were higher than AAV-EGFP -control group (1 vs. 1.35, P<0.01). There was no significant difference between AAV-C-ΔWD7 treated group and control group (1 vs. 1.02). Control, n=9 mice; AAV-NRIP treatment, N=8 mice; AAV-NRIP-C treatment, n=3 mice; AAV-C-ΔWD7 treatment, n=2 mice. Data are mean ± SEM by two tailed Student's t-test. *P<0.05, **P<0.01 and ***P<0.001.

doi:10.6342/NTU201902676

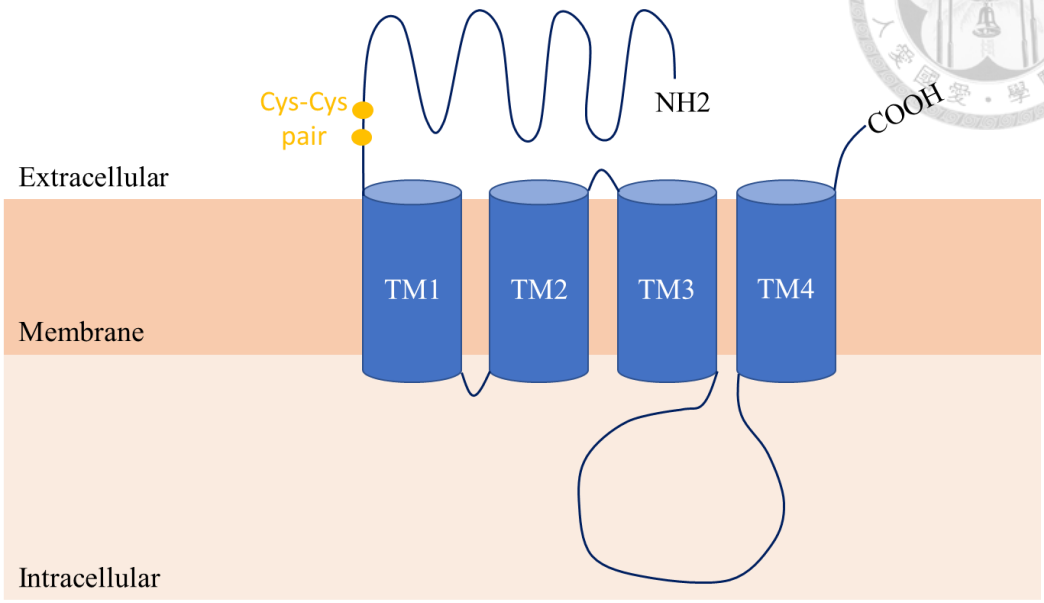

Supplementary Fig. S1. Schematic presentation of acetylcholine receptor (AChR) subunit structure.

Acetylcholine receptor (AChR) consist of 4 subunits - α, β, γ, δ and assembles into a pentamer as $\alpha_2\beta\gamma\delta$. All subunits have four common structural domains: (1) ~200 amino acid of conserved extracellular large NH2-terminal domain; (2) three prominent and conserved transmembrane (TM) domain; (3) one cytoplasmic loop with variable size and amino acid sequence; (4) a fourth TM domain with a relatively short and variable extracellular COOH-terminal sequence. Four subunits are further classified to α- and non α- subunits depending on presence of a cysteine–cysteine (Cys-Cys) pair, which is required for agonist binding, near the entrance of TM1. Subunits with presence of Cys-Cys pair would be identified as α- subunit.

doi:10.6342/NTU201902676

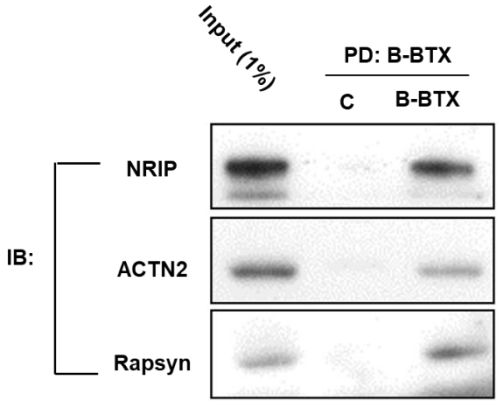

Supplementary Fig. S2. NRIP is a novel structural component of AChR complex. (A,B: Yun-Hsin Huang unpublished data; C: Hsin-Hsiung Chen unpublished data) NRIP is a novel protein in AChR complex. Gastrocnemius muscles protein lysates were incubated with biotin-labeled BTX (B-BTX), then pulled down by streptavidin-coupled agarose beads. C, control, was streptavidin-coupled agarose beads only. NRIP is included in the pulled down protein with ACTN2 and rapsyn, indicates that NRIP is one of the AChR complex protein.

doi:10.6342/NTU201902676

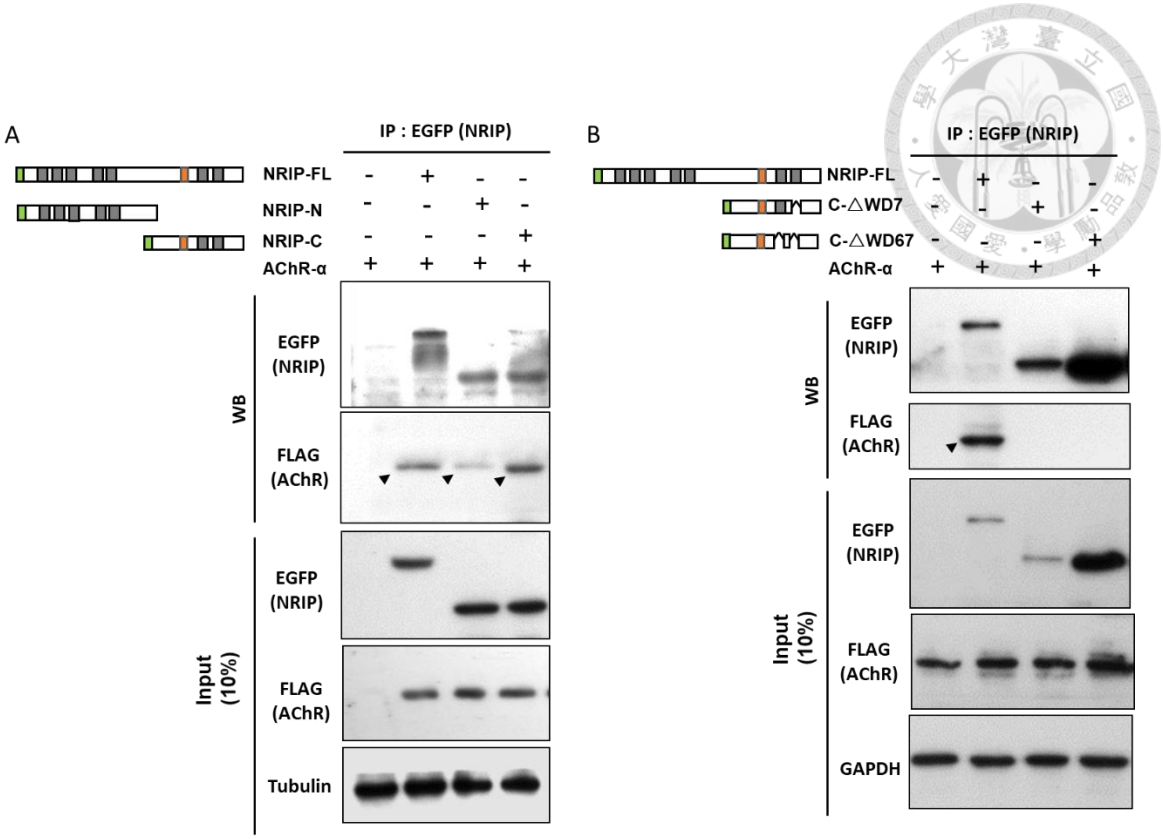

Supplementary Fig. S3. The interaction of NRIP mutants and AChR-α.
(Hsin-Hsiung Chen unpublished data)

(A) AChR α has decreased binding with NRIP-N. Immunoprecipitation assay for AChR-α binding with NRIP mutants. HEK293T cells were transfected with Flag-AChR-α and EGFP-NRIP mutants. Flag-AChR-α were purified by IP with anti-EGFP antibody and showed by anti-FLAG antibody. Anti-tubulin used as internal control. Arrow head indicates AChR α nteraction with NRIP mutant protein. (B) C-ΔWD67 and C-ΔWD7 loss AChR α binding. Immunoprecipitation assay for AChR-α binding with NRIP mutants. HEK293T cells were transfected with Flag-AChR-α and EGFP-NRIP mutants. Flag-AChR-α were purified by IP with anti-EGFP antibody and showed by anti-FLAG antibody. Anti- GAPDH used as internal control. Arrow head indicates AChR α has interaction with NRIP mutant protein.

doi:10.6342/NTU201902676

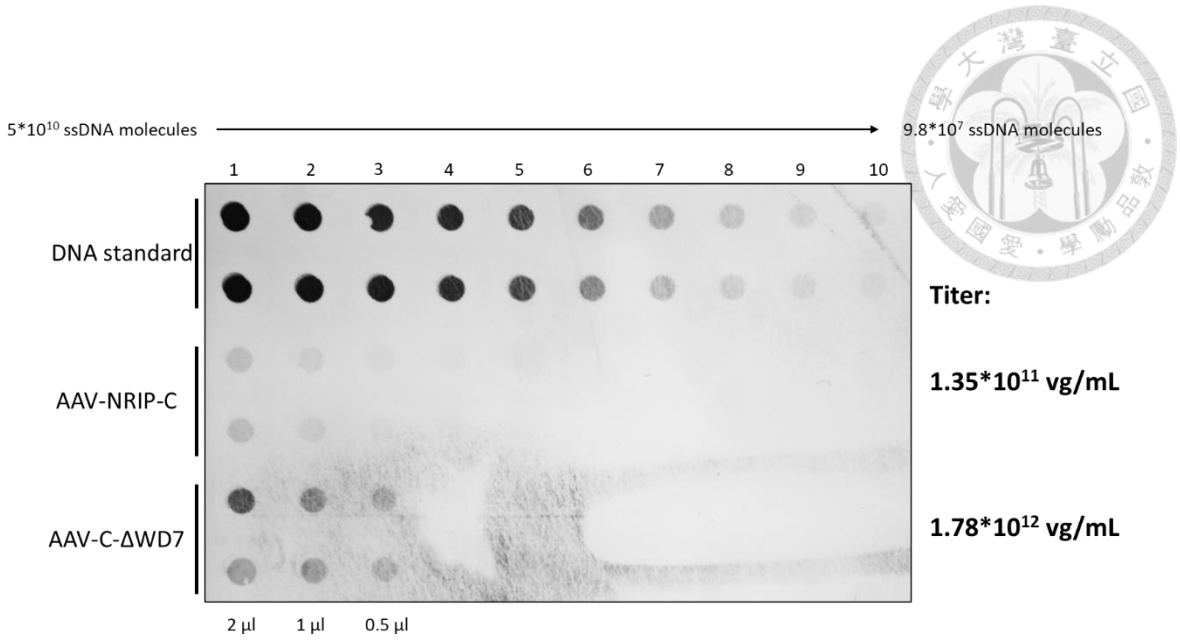

Supplementary Fig.S4. The dot blot assay for adeno-associated virus (AAV) titration. The dot blot was done by Yi-Hsiang Liu. Dot blot assay was used to calculate rAAV titers. DNA standard ranged from $5*10^{10}$ to $9.8*10^{7}$ single-stranded DNA were linearized and denatured form the plasmid AAV-EGFP construct as positive control. Two repetitions of five 2-fold serial dilutions of AAV-NRIP-C and AAV- C-ΔWD7 were loaded and the signals were analyzed by ImageJ software. The titers of AAV-NRIP-C were $1.35*10^{11}$ vg/mL, and the titer of AAV-C-ΔWD7 were $1.78*10^{12}$ vg/mL.

doi:10.6342/NTU201902676

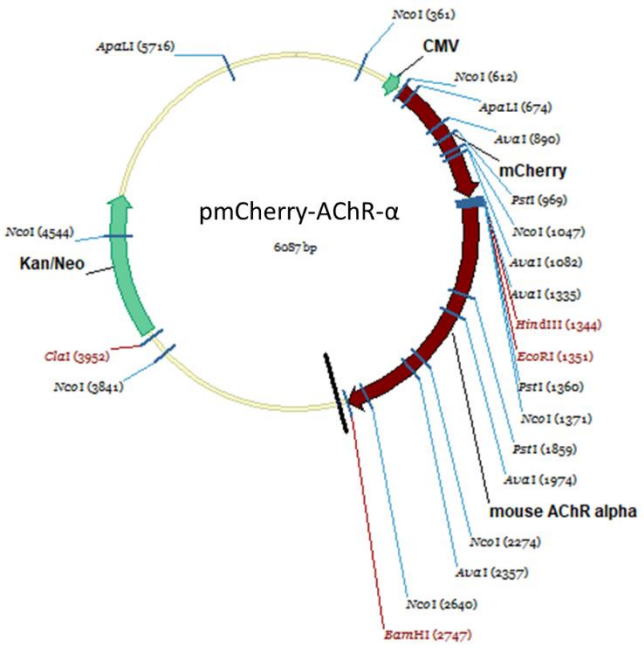

Supplementary Fig.S5. Plasmid map of pmCherry-AChR-α.
(constructed by Hsin-Hsiung Chen)

The insert DNA-AChR-α were amplified from the template of FLAG-AChR-α (plasmid from Lin Mei's Lab (Li et al., 2016)) by PCR, using primer as follows (5' to 3'): TGA AGC TTC CAT GGA GCT CTC (*CHRNA* forward), AAG GAT CCT CAT CCT TGT TGA TC (*CHRNA* reverse). For cloning, KpnI and BamHI enzyme site located on pmCherry multiple cloning sites (MCS) were used.

doi:10.6342/NTU201902676

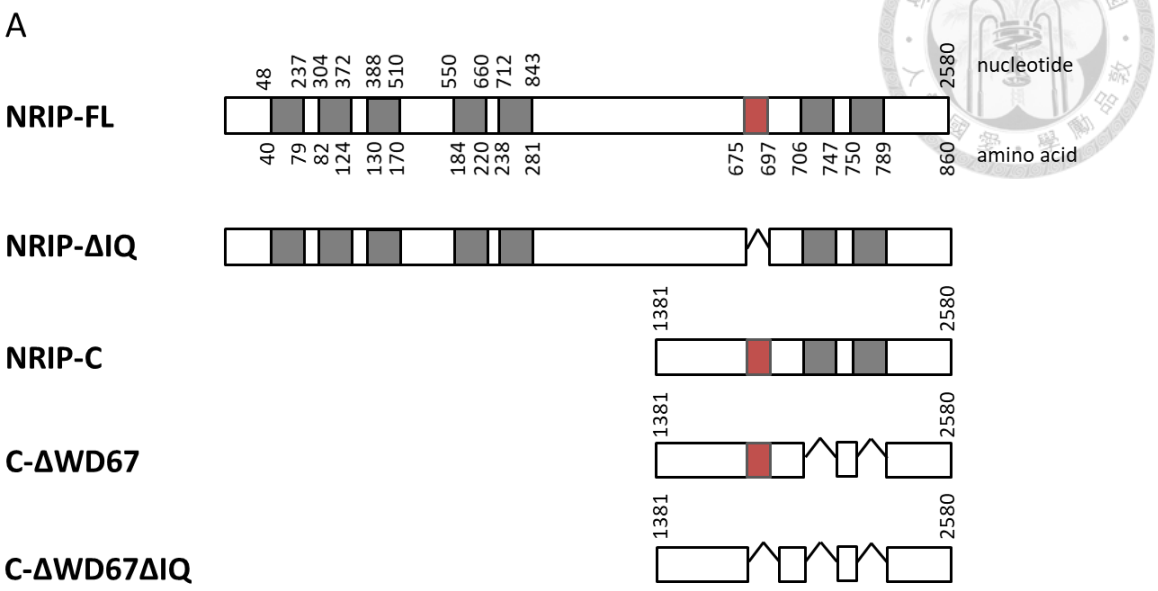

Supplementary Fig.S6. Schematic illustration of NRIP truncated mutants with nucleotide and amino acid numbers
(Scheme by Ya-Ju Han)

doi:10.6342/NTU201902676

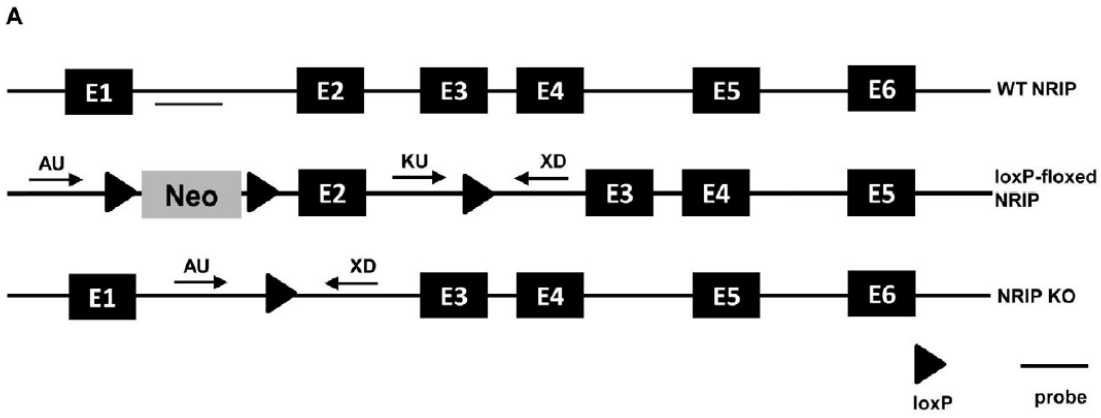

Appendix Fig.1 generation of muscle-specific NRIP knockout (cKO) mice.
Schematic illustration of genomic structure of wild-type (WT) NRIP, *loxP*-floxed NRIP, and NRIP-deleted alleles (Chen et al., 2015). The *loxP*-floxed allele contains a neo cassette with two flanked loxP sequences in intron 1 and a loxP sequence in intron 2. NRIP exon 2 would be deleted by Cre recombinase driven by *MCK* promoter.

doi:10.6342/NTU201902676

Primers for Cre recombinase genotyping	
Primer name	Primer Sequence (5’ to 3’)
oIMR1580	GTGAAACAGCATTGCTGTCACTT
oIMR6754	TAAGTCTGAACCCGGTCTGC
oIMR8744	CAAATGTTGCTTGTCTGGTG
oIMR8745	GTCAGTCGAGTGCACAGTTT
Primers for pmCherry-AChR-α construction	
Primer name	Primer Sequence (5’ to 3’)
CHRNA forward	TGAAGCTTCCATGGAGCTCTC
CHRNA reverse	AAGGATCCTCATCCTTGTTGATC

Appendix Fig.2 Primer sequences.

Plasmid name	Plasmid backbone
NRIP-FL	pEGFP-N1
NRIP-C	pEGFP-N1
NRIP-N	pEGFP-N1
NRIP-ΔIQ	pEGFP-N1
C-ΔWD7	pEGFP-N1
mCherry-AChR-α	pmCherry-N1
AAV-NRIP-C	pAAV-MCS
AAV- C-ΔWD7	pAAV-MCS

Appendix Fig.3 Plasmid backbones list.

doi:10.6342/NTU201902676

Cell staining			
Antibody name	company	Cat No.	Dilution
Wheat germ agglutinin (WGA)-555 conjugate	ThermoFisher	W32464	1:200
Calnexin	abcam	ab22595	1:200
Flag	Sigma	F3165	1:200
GFP	Santa Cruz	sc-9996	1:50
Western blot			
Antibody name	company	Cat No.	Dilution
EGFP	abcam	ab183734	1:10000
Flag	Sigma	F3165	1:10000
GAPDH	AbFrontier	LF-PA0212	1:10000
Tissue staining			
Antibody name	company	Cat No.	Dilution
EGFP	abcam	ab183734	1:200
Alexa-594-conjugated α-bungarotoxin	Life techologies	B13423	1:1000
Neurofilament	abcam	ab8135	1:500
synaptophysin	abcam	Ab32127	1:250
NeuN	Millipore	MABN140	1:500
ChAT	Millipore	AB144P	1:250

Appendix Fig.4 Antibody lists.

doi:10.6342/NTU201902676

Chapter 8 References

Adams, M.E., Kramarcy, N., Krall, S.P., Rossi, S.G., Rotundo, R.L., Sealock, R., and Froehner, S.C. (2000). Absence of alpha-syntrophin leads to structurally aberrant neuromuscular synapses deficient in utrophin. J Cell Biol *150*, 1385-1398.

Aittaleb, M., Martinez-Pena, Y.V.I., and Akaaboune, M. (2017). Spatial distribution and molecular dynamics of dystrophin glycoprotein components at the neuromuscular junction in vivo. J Cell Sci *130*, 1752-1759.

Albuquerque, E.X., Pereira, E.F., Alkondon, M., and Rogers, S.W. (2009). Mammalian nicotinic acetylcholine receptors: from structure to function. Physiol Rev *89*, 73-120.

Antolik, C., Catino, D.H., O'Neill, A.M., Resneck, W.G., Ursitti, J.A., and Bloch, R.J. (2007). The actin binding domain of ACF7 binds directly to the tetratricopeptide repeat domains of rapsyn. Neuroscience *145*, 56-65.

Apel, E.D., Glass, D.J., Moscoso, L.M., Yancopoulos, G.D., and Sanes, J.R. (1997). Rapsyn is required for MuSK signaling and recruits synaptic components to a MuSK-containing scaffold. Neuron *18*, 623-635.

Bahler, M., and Rhoads, A. (2002). Calmodulin signaling via the IQ motif. FEBS Lett *513*, 107-113.

Banks, G.B., Chau, T.N., Bartlett, S.E., and Noakes, P.G. (2001). Promotion of motoneuron survival and branching in rapsyn-deficient mice. J Comp Neurol *429*, 156-165.

Barnard, E.A., Coates, V., Dolly, J.O., and Mallick, B. (1977). Binding of alpha-bungarotoxin and cholinergic ligands to acetylcholine receptors in the membrane of skeletal muscle. Cell Biol Int Rep *1*, 99-106.

Bartoli, M., Ramarao, M.K., and Cohen, J.B. (2001). Interactions of the rapsyn RING-H2 domain with dystroglycan. J Biol Chem *276*, 24911-24917.

Berrih-Aknin, S., Frenkian-Cuvelier, M., and Eymard, B. (2014). Diagnostic and clinical classification of autoimmune myasthenia gravis. J Autoimmun *48-49*, 143-148.

doi:10.6342/NTU201902676

Bhattacharya, S., Bunick, C.G., and Chazin, W.J. (2004). Target selectivity in EF-hand calcium binding proteins. Biochim Biophys Acta *1742*, 69-79.

Blake, D.J., Weir, A., Newey, S.E., and Davies, K.E. (2002). Function and genetics of dystrophin and dystrophin-related proteins in muscle. Physiol Rev *82*, 291-329.

Boillee, S., and Cleveland, D.W. (2004). Gene therapy for ALS delivers. Trends Neurosci *27*, 235-238.

Borges, L.S., Yechikhov, S., Lee, Y.I., Rudell, J.B., Friese, M.B., Burden, S.J., and Ferns, M.J. (2008). Identification of a motif in the acetylcholine receptor beta subunit whose phosphorylation regulates rapsyn association and postsynaptic receptor localization. J Neurosci *28*, 11468-11476.

Brockhausen, J., Cole, R.N., Gervasio, O.L., Ngo, S.T., Noakes, P.G., and Phillips, W.D. (2008). Neural agrin increases postsynaptic ACh receptor packing by elevating rapsyn protein at the mouse neuromuscular synapse. Dev Neurobiol *68*, 1153-1169.

Bruneau, E.G., and Akaaboune, M. (2006). The dynamics of recycled acetylcholine receptors at the neuromuscular junction in vivo. Development *133*, 4485-4493.

Bruning, J.C., Michael, M.D., Winnay, J.N., Hayashi, T., Horsch, D., Accili, D., Goodyear, L.J., and Kahn, C.R. (1998). A muscle-specific insulin receptor knockout exhibits features of the metabolic syndrome of NIDDM without altering glucose tolerance. Mol Cell *2*, 559-569.

Burden, S.J., Huijbers, M.G., and Remedio, L. (2018). Fundamental Molecules and Mechanisms for Forming and Maintaining Neuromuscular Synapses. Int J Mol Sci *19*.

Calabria, E., Ciciliot, S., Moretti, I., Garcia, M., Picard, A., Dyar, K.A., Pallafacchina, G., Tothova, J., Schiaffino, S., and Murgia, M. (2009). NFAT isoforms control activity-dependent muscle fiber type specification. Proc Natl Acad Sci U S A *106*, 13335-13340.

Cary, G.A., and La Spada, A.R. (2008). Androgen receptor function in motor neuron survival and degeneration. Phys Med Rehabil Clin N Am *19*, 479-494, viii.

Chang, S.W., Tsao, Y.P., Lin, C.Y., and Chen, S.L. (2011). NRIP, a novel calmodulin binding protein, activates calcineurin to dephosphorylate human papillomavirus E2

doi:10.6342/NTU201902676

protein. J Virol *85*, 6750-6763.

Chen, H.H., Chen, W.P., Yan, W.L., Huang, Y.C., Chang, S.W., Fu, W.M., Su, M.J., Yu, I.S., Tsai, T.C., Yan, Y.T., *et al.* (2015). NRIP is newly identified as a Z-disc protein, activating calmodulin signaling for skeletal muscle contraction and regeneration. J Cell Sci *128*, 4196-4209.

Chen, H.H., Fan, P., Chang, S.W., Tsao, Y.P., Huang, H.P., and Chen, S.L. (2017). NRIP/DCAF6 stabilizes the androgen receptor protein by displacing DDB2 from the CUL4A-DDB1 E3 ligase complex in prostate cancer. Oncotarget *8*, 21501-21515.

Chen, H.H., Tsai, L.K., Liao, K.Y., Wu, T.C., Huang, Y.H., Huang, Y.C., Chang, S.W., Wang, P.Y., Tsao, Y.P., and Chen, S.L. (2018). Muscle-restricted nuclear receptor interaction protein knockout causes motor neuron degeneration through down-regulation of myogenin at the neuromuscular junction. J Cachexia Sarcopenia Muscle *9*, 771-785.

Chen, P.H., Tsao, Y.P., Wang, C.C., and Chen, S.L. (2008). Nuclear receptor interaction protein, a coactivator of androgen receptors (AR), is regulated by AR and Sp1 to feed forward and activate its own gene expression through AR protein stability. Nucleic Acids Res *36*, 51-66.

Chen, P.J., Martinez-Pena, Y.V.I., Aittaleb, M., and Akaaboune, M. (2016). AChRs Are Essential for the Targeting of Rapsyn to the Postsynaptic Membrane of NMJs in Living Mice. J Neurosci *36*, 5680-5685.

Chen, Y., Ip, F.C., Shi, L., Zhang, Z., Tang, H., Ng, Y.P., Ye, W.C., Fu, A.K., and Ip, N.Y. (2014). Coronin 6 regulates acetylcholine receptor clustering through modulating receptor anchorage to actin cytoskeleton. J Neurosci *34*, 2413-2421.

Cheung, C.L., Chan, B.Y., Chan, V., Ikegawa, S., Kou, I., Ngai, H., Smith, D., Luk, K.D., Huang, Q.Y., Mori, S., *et al.* (2009). Pre-B-cell leukemia homeobox 1 (PBX1) shows functional and possible genetic association with bone mineral density variation. Hum Mol Genet *18*, 679-687.

Chin, E.R., Olson, E.N., Richardson, J.A., Yang, Q., Humphries, C., Shelton, J.M., Wu, H., Zhu, W., Bassel-Duby, R., and Williams, R.S. (1998). A calcineurin-dependent transcriptional pathway controls skeletal muscle fiber type. Genes Dev *12*, 2499-2509.

doi:10.6342/NTU201902676

Chou, H.J., Lai, D.M., Huang, C.W., McLennan, I.S., Wang, H.D., and Wang, P.Y. (2013). BMP4 is a peripherally-derived factor for motor neurons and attenuates glutamate-induced excitotoxicity in vitro. PLoS One *8*, e58441.

Cohen, J.B., Weber, M., Huchet, M., and Changeux, J.P. (1972). Purification from Torpedo marmorata electric tissue of membrane fragments particularly rich in cholinergic receptor protein. FEBS Lett *26*, 43-47.

DeChiara, T.M., Bowen, D.C., Valenzuela, D.M., Simmons, M.V., Poueymirou, W.T., Thomas, S., Kinetz, E., Compton, D.L., Rojas, E., Park, J.S.*, et al.* (1996). The receptor tyrosine kinase MuSK is required for neuromuscular junction formation in vivo. Cell *85*, 501-512.

Dobbins, G.C., Luo, S., Yang, Z., Xiong, W.C., and Mei, L. (2008). alpha-Actinin interacts with rapsyn in agrin-stimulated AChR clustering. Mol Brain *1*, 18.

Drachman, D.B., Angus, C.W., Adams, R.N., and Kao, I. (1978). Effect of myasthenic patients' immunoglobulin on acetylcholine receptor turnover: selectivity of degradation process. Proc Natl Acad Sci U S A *75*, 3422-3426.

Ehret, G.B., O'Connor, A.A., Weder, A., Cooper, R.S., and Chakravarti, A. (2009). Follow-up of a major linkage peak on chromosome 1 reveals suggestive QTLs associated with essential hypertension: GenNet study. Eur J Hum Genet *17*, 1650-1657.

Engel, A.G., Shen, X.M., Selcen, D., and Sine, S.M. (2015). Congenital myasthenic syndromes: pathogenesis, diagnosis, and treatment. Lancet Neurol *14*, 420-434.

Froehner, S.C., Luetje, C.W., Scotland, P.B., and Patrick, J. (1990). The postsynaptic 43K protein clusters muscle nicotinic acetylcholine receptors in Xenopus oocytes. Neuron *5*, 403-410.

Funakoshi, H., Belluardo, N., Arenas, E., Yamamoto, Y., Casabona, A., Persson, H., and Ibanez, C.F. (1995). Muscle-derived neurotrophin-4 as an activity-dependent trophic signal for adult motor neurons. Science *268*, 1495-1499.

Gilhus, N.E., and Verschuuren, J.J. (2015). Myasthenia gravis: subgroup classification and therapeutic strategies. Lancet Neurol *14*, 1023-1036.

doi:10.6342/NTU201902676

Green, W.N., and Claudio, T. (1993). Acetylcholine receptor assembly: subunit folding and oligomerization occur sequentially. Cell *74*, 57-69.

Han, C.P., Lee, M.Y., Tzeng, S.L., Yao, C.C., Wang, P.H., Cheng, Y.W., Chen, S.L., Wu, T.S., Tyan, Y.S., and Kok, L.F. (2008). Nuclear Receptor Interaction Protein (NRIP) expression assay using human tissue microarray and immunohistochemistry technology confirming nuclear localization. J Exp Clin Cancer Res *27*, 25.

Heiska, L., Kantor, C., Parr, T., Critchley, D.R., Vilja, P., Gahmberg, C.G., and Carpen, O. (1996). Binding of the cytoplasmic domain of intercellular adhesion molecule-2 (ICAM-2) to alpha-actinin. J Biol Chem *271*, 26214-26219.

Huze, C., Bauche, S., Richard, P., Chevessier, F., Goillot, E., Gaudon, K., Ben Ammar, A., Chaboud, A., Grosjean, I., Lecuyer, H.A.*, et al.* (2009). Identification of an agrin mutation that causes congenital myasthenia and affects synapse function. Am J Hum Genet *85*, 155-167.

Jin, J., Arias, E.E., Chen, J., Harper, J.W., and Walter, J.C. (2006). A family of diverse Cul4-Ddb1-interacting proteins includes Cdt2, which is required for S phase destruction of the replication factor Cdt1. Mol Cell *23*, 709-721.

Kanning, K.C., Kaplan, A., and Henderson, C.E. (2010). Motor neuron diversity in development and disease. Annu Rev Neurosci *33*, 409-440.

Kim, N., Stiegler, A.L., Cameron, T.O., Hallock, P.T., Gomez, A.M., Huang, J.H., Hubbard, S.R., Dustin, M.L., and Burden, S.J. (2008). Lrp4 is a receptor for Agrin and forms a complex with MuSK. Cell *135*, 334-342.

Kracun, S., Harkness, P.C., Gibb, A.J., and Millar, N.S. (2008). Influence of the M3-M4 intracellular domain upon nicotinic acetylcholine receptor assembly, targeting and function. Br J Pharmacol *153*, 1474-1484.

Le Novere, N., Corringer, P.J., and Changeux, J.P. (1999). Improved secondary structure predictions for a nicotinic receptor subunit: incorporation of solvent accessibility and experimental data into a two-dimensional representation. Biophys J *76*, 2329-2345.

Lee, Y., Rudell, J., and Ferns, M. (2009). Rapsyn interacts with the muscle acetylcholine receptor via alpha-helical domains in the alpha, beta, and epsilon subunit intracellular

doi:10.6342/NTU201902676

loops. Neuroscience *163*, 222-232.

Li, L., Cao, Y., Wu, H., Ye, X., Zhu, Z., Xing, G., Shen, C., Barik, A., Zhang, B., Xie, X., *et al.* (2016). Enzymatic Activity of the Scaffold Protein Rapsyn for Synapse Formation. Neuron *92*, 1007-1019.

Lin, W., Burgess, R.W., Dominguez, B., Pfaff, S.L., Sanes, J.R., and Lee, K.F. (2001). Distinct roles of nerve and muscle in postsynaptic differentiation of the neuromuscular synapse. Nature *410*, 1057-1064.

Marchand, S., Bignami, F., Stetzkowski-Marden, F., and Cartaud, J. (2000). The myristoylated protein rapsyn is cotargeted with the nicotinic acetylcholine receptor to the postsynaptic membrane via the exocytic pathway. J Neurosci *20*, 521-528.

Marchand, S., Devillers-Thiery, A., Pons, S., Changeux, J.P., and Cartaud, J. (2002). Rapsyn escorts the nicotinic acetylcholine receptor along the exocytic pathway via association with lipid rafts. J Neurosci *22*, 8891-8901.

Marques, M.J., Conchello, J.A., and Lichtman, J.W. (2000). From plaque to pretzel: fold formation and acetylcholine receptor loss at the developing neuromuscular junction. J Neurosci *20*, 3663-3675.

Martinez-Pena y Valenzuela, I., Mouslim, C., Pires-Oliveira, M., Adams, M.E., Froehner, S.C., and Akaaboune, M. (2011). Nicotinic acetylcholine receptor stability at the NMJ deficient in alpha-syntrophin in vivo. J Neurosci *31*, 15586-15596.

Maselli, R.A., Arredondo, J., Cagney, O., Ng, J.J., Anderson, J.A., Williams, C., Gerke, B.J., Soliven, B., and Wollmann, R.L. (2010). Mutations in MUSK causing congenital myasthenic syndrome impair MuSK-Dok-7 interaction. Hum Mol Genet *19*, 2370-2379.

Mills, M., Yang, N., Weinberger, R., Vander Woude, D.L., Beggs, A.H., Easteal, S., and North, K. (2001). Differential expression of the actin-binding proteins, alpha-actinin-2 and -3, in different species: implications for the evolution of functional redundancy. Hum Mol Genet *10*, 1335-1346.

Misawa, H., Hara, M., Tanabe, S., Niikura, M., Moriwaki, Y., and Okuda, T. (2012). Osteopontin is an alpha motor neuron marker in the mouse spinal cord. J Neurosci Res *90*, 732-742.

doi:10.6342/NTU201902676

Moransard, M., Borges, L.S., Willmann, R., Marangi, P.A., Brenner, H.R., Ferns, M.J., and Fuhrer, C. (2003). Agrin regulates rapsyn interaction with surface acetylcholine receptors, and this underlies cytoskeletal anchoring and clustering. J Biol Chem *278*, 7350-7359.

Musil, L.S., Carr, C., Cohen, J.B., and Merlie, J.P. (1988). Acetylcholine receptor-associated 43K protein contains covalently bound myristate. J Cell Biol *107*, 1113-1121.

Nakano, K., Miki, Y., Hata, S., Ebata, A., Takagi, K., McNamara, K.M., Sakurai, M., Masuda, M., Hirakawa, H., Ishida, T.*, et al.* (2013). Identification of androgen-responsive microRNAs and androgen-related genes in breast cancer. Anticancer Res *33*, 4811-4819.

Neubig, R.R., Krodel, E.K., Boyd, N.D., and Cohen, J.B. (1979). Acetylcholine and local anesthetic binding to Torpedo nicotinic postsynaptic membranes after removal of nonreceptor peptides. Proc Natl Acad Sci U S A *76*, 690-694.

Noakes, P.G., Phillips, W.D., Hanley, T.A., Sanes, J.R., and Merlie, J.P. (1993). 43K protein and acetylcholine receptors colocalize during the initial stages of neuromuscular synapse formation in vivo. Dev Biol *155*, 275-280.

Ohkawara, B., Cabrera-Serrano, M., Nakata, T., Milone, M., Asai, N., Ito, K., Ito, M., Masuda, A., Ito, Y., Engel, A.G.*, et al.* (2014). LRP4 third beta-propeller domain mutations cause novel congenital myasthenia by compromising agrin-mediated MuSK signaling in a position-specific manner. Hum Mol Genet *23*, 1856-1868.

Ohno, K., Engel, A.G., Shen, X.M., Selcen, D., Brengman, J., Harper, C.M., Tsujino, A., and Milone, M. (2002). Rapsyn mutations in humans cause endplate acetylcholine-receptor deficiency and myasthenic syndrome. Am J Hum Genet *70*, 875-885.

Otey, C.A., and Carpen, O. (2004). Alpha-actinin revisited: a fresh look at an old player. Cell Motil Cytoskeleton *58*, 104-111.

Oury, J., Liu, Y., Topf, A., Todorovic, S., Hoedt, E., Preethish-Kumar, V., Neubert, T.A., Lin, W., Lochmuller, H., and Burden, S.J. (2019). MACF1 links Rapsyn to microtubule- and actin-binding proteins to maintain neuromuscular synapses. J Cell Biol *218*, 1686-1705.

doi:10.6342/NTU201902676

Park, K.H., Franciosi, S., and Leavitt, B.R. (2013). Postnatal muscle modification by myogenic factors modulates neuropathology and survival in an ALS mouse model. Nat Commun *4*, 2906.

Pawlikowski, B.T., and Maimone, M.M. (2009). Formation of complex AChR aggregates in vitro requires alpha-dystrobrevin. Dev Neurobiol *69*, 326-338.

Phillips, W.D., Kopta, C., Blount, P., Gardner, P.D., Steinbach, J.H., and Merlie, J.P. (1991). ACh receptor-rich membrane domains organized in fibroblasts by recombinant 43-kildalton protein. Science *251*, 568-570.

Ramarao, M.K., Bianchetta, M.J., Lanken, J., and Cohen, J.B. (2001). Role of rapsyn tetratricopeptide repeat and coiled-coil domains in self-association and nicotinic acetylcholine receptor clustering. J Biol Chem *276*, 7475-7483.

Ramarao, M.K., and Cohen, J.B. (1998). Mechanism of nicotinic acetylcholine receptor cluster formation by rapsyn. Proc Natl Acad Sci U S A *95*, 4007-4012.

Rhoads, A.R., and Friedberg, F. (1997). Sequence motifs for calmodulin recognition. FASEB J *11*, 331-340.

Sanes, J.R., and Lichtman, J.W. (1999). Development of the vertebrate neuromuscular junction. Annu Rev Neurosci *22*, 389-442.

Shi, Y., Li, Z., Xu, Q., Wang, T., Li, T., Shen, J., Zhang, F., Chen, J., Zhou, G., Ji, W.*, et al.* (2011). Common variants on 8p12 and 1q24.2 confer risk of schizophrenia. Nat Genet *43*, 1224-1227.

Sjoblom, B., Salmazo, A., and Djinovic-Carugo, K. (2008). Alpha-actinin structure and regulation. Cell Mol Life Sci *65*, 2688-2701.

Sobel, A., Weber, M., and Changeux, J.P. (1977). Large-scale purification of the acetylcholine-receptor protein in its membrane-bound and detergent-extracted forms from Torpedo marmorata electric organ. Eur J Biochem *80*, 215-224.

Steinbach, J.H. (1981). Developmental changes in acetylcholine receptor aggregates at rat skeletal neuromuscular junctions. Dev Biol *84*, 267-276.

doi:10.6342/NTU201902676

Stirnimann, C.U., Petsalaki, E., Russell, R.B., and Muller, C.W. (2010). WD40 proteins propel cellular networks. Trends Biochem Sci *35*, 565-574.

Tintignac, L.A., Brenner, H.R., and Ruegg, M.A. (2015). Mechanisms Regulating Neuromuscular Junction Development and Function and Causes of Muscle Wasting. Physiol Rev *95*, 809-852.

Tsai, T.C., Lee, Y.L., Hsiao, W.C., Tsao, Y.P., and Chen, S.L. (2005). NRIP, a novel nuclear receptor interaction protein, enhances the transcriptional activity of nuclear receptors. J Biol Chem *280*, 20000-20009.

Tse, N., Morsch, M., Ghazanfari, N., Cole, L., Visvanathan, A., Leamey, C., and Phillips, W.D. (2014). The neuromuscular junction: measuring synapse size, fragmentation and changes in synaptic protein density using confocal fluorescence microscopy. J Vis Exp.

Tsitkanou, S., Della Gatta, P.A., and Russell, A.P. (2016). Skeletal Muscle Satellite Cells, Mitochondria, and MicroRNAs: Their Involvement in the Pathogenesis of ALS. Front Physiol *7*, 403.

Unwin, N. (2005). Refined structure of the nicotinic acetylcholine receptor at 4A resolution. J Mol Biol *346*, 967-989.

Unwin, N. (2013). Nicotinic acetylcholine receptor and the structural basis of neuromuscular transmission: insights from Torpedo postsynaptic membranes. Q Rev Biophys *46*, 283-322.

Valenzuela, D.M., Stitt, T.N., DiStefano, P.S., Rojas, E., Mattsson, K., Compton, D.L., Nunez, L., Park, J.S., Stark, J.L., Gies, D.R.*, et al.* (1995). Receptor tyrosine kinase specific for the skeletal muscle lineage: expression in embryonic muscle, at the neuromuscular junction, and after injury. Neuron *15*, 573-584.

Walikonis, R.S., Oguni, A., Khorosheva, E.M., Jeng, C.J., Asuncion, F.J., and Kennedy, M.B. (2001). Densin-180 forms a ternary complex with the (alpha)-subunit of Ca2+/calmodulin-dependent protein kinase II and (alpha)-actinin. J Neurosci *21*, 423-433.

Wanamaker, C.P., Christianson, J.C., and Green, W.N. (2003). Regulation of nicotinic acetylcholine receptor assembly. Ann N Y Acad Sci *998*, 66-80.

doi:10.6342/NTU201902676

Wang, J., Jing, Z., Zhang, L., Zhou, G., Braun, J., Yao, Y., and Wang, Z.Z. (2003). Regulation of acetylcholine receptor clustering by the tumor suppressor APC. Nat Neurosci *6*, 1017-1018.

Wu, H., Xiong, W.C., and Mei, L. (2010). To build a synapse: signaling pathways in neuromuscular junction assembly. Development *137*, 1017-1033.

Xu, C., and Min, J. (2011). Structure and function of WD40 domain proteins. Protein Cell *2*, 202-214.

Yu, X.M., and Hall, Z.W. (1994). The role of the cytoplasmic domains of individual subunits of the acetylcholine receptor in 43 kDa protein-induced clustering in COS cells. J Neurosci *14*, 785-795.

Zhang, B., Luo, S., Dong, X.P., Zhang, X., Liu, C., Luo, Z., Xiong, W.C., and Mei, L. (2007). Beta-catenin regulates acetylcholine receptor clustering in muscle cells through interaction with rapsyn. J Neurosci *27*, 3968-3973.

Zhou, H., Glass, D.J., Yancopoulos, G.D., and Sanes, J.R. (1999). Distinct domains of MuSK mediate its abilities to induce and to associate with postsynaptic specializations. J Cell Biol *146*, 1133-1146.

Ziskind-Conhaim, L., and Bennett, J.I. (1982). The effects of electrical inactivity and denervation on the distribution of acetylcholine receptors in developing rat muscle. Dev Biol *90*, 185-197.

doi:10.6342/NTU201902676